

A posteriori analysis of a virtual element approach on polytopal meshes for the buckling eigenvalue problem

Franco Dassi^a, Andrés E. Rubiano^b, Iván Velásquez^c

^a*Dipartimento di Matematica e Applicazioni, Università degli studi di Milano Bicocca, Via Roberto Cozzi 55 - 20125 Milano, Italy.*

^b*School of Mathematics, Monash University, 9 Rainforest Walk, Melbourne, VIC 3800, Australia.*

^c*Departamento de Matemáticas, Universidad Militar Nueva Granada, Bogotá, Colombia.*

Abstract

We introduce a novel residual-based a posteriori error estimator for the conforming C^1 Virtual Element Method (VEM) applied to the buckling eigenvalue problem, incorporating nonlinear plane stress effects in both two and three dimensions. The estimator is fully computable on general polyhedral meshes and implemented within the open-source `vem++` library. Its reliability is rigorously justified via bounds on the residual equation using polynomial projections, stabilisation contributions, and interpolation estimates, while efficiency is ensured through the use of bubble function arguments. Comprehensive numerical experiments in 2D and 3D illustrate the estimator's optimal accuracy and robustness, highlighting its potential for predictive analysis of complex plate structures.

Keywords: A posteriori error analysis in 2D and 3D, virtual element method, buckling spectral problem.

1. Introduction

The instability of thin plates under in-plane loading can be formulated as a buckling eigenvalue problem for the transverse displacement of the plate. The governing equation involves the fourth-order bending operator together with additional terms accounting for the effect of the (possibly nonlinear) in-plane stresses on the deflection. In this formulation, the eigenvalue represents a critical load parameter rather than a vibration frequency. Buckling occurs when the load reaches values for which the homogeneous problem admits nontrivial solutions. The corresponding eigenfunctions describe the buckling modes, while the smallest eigenvalue determines the first buckling load, marking the loss of stability of the flat configuration. This class of problems has attracted significant attention due to its importance in engineering applications, such as the design of automotive, underwater and aerospace structures, where predicting instability is crucial for safety and performance (e.g. [10, 36]).

Email addresses: `franco.dassi@unimib.it` (Franco Dassi), `andres.rubianomartinez@monash.edu` (Andrés E. Rubiano), `ivan.velasquez@unimilitar.edu.co` (Iván Velásquez)

Several numerical methods have been proposed for the approximation of the buckling eigenvalue problem, including conforming, nonconforming, and mixed Finite Element Method (FEM) and Virtual Element Method (VEM) discretisations, as well as discrete singular convolution (DSC) methods. We refer to [1, 7, 11, 14, 24, 26, 28, 31] for a non-exhaustive list of contributions on this topic.

In this work, we employ a conforming VEM for the H^2 variational formulation of the buckling eigenvalue problem [3, 6]. Unlike classical C^1 FEM (see e.g. [13]), which typically require high polynomial degrees and a large number of degrees of freedom (DoFs) to ensure conformity, the lowest-order conforming VEM achieves this with significantly fewer DoFs —specifically, 3 per vertex in 2D and 4 per vertex in 3D. Furthermore, the VEM naturally accommodates general polyhedral elements, including non-convex shapes, and efficiently handles hanging nodes, simplifying the implementation of adaptive refinement strategies.

A posteriori error estimation plays a central role in the numerical approximation of Partial Differential Equations (PDEs), particularly when the exact solution is unknown. These estimators are computable quantities that depend only on the discrete solution and the problem data, which provide practical information about the quality of a given numerical approximation. In particular, adaptive schemes use a posteriori error estimators to identify regions of the computational domain where the error is large, which enables a selective refinement of the mesh that leads to more efficient algorithms that concentrate computational effort where it is most needed. This is particularly relevant for problems exhibiting localised phenomena, such as boundary layers, singularities, or sharp gradients.

From a mathematical viewpoint, an a posteriori error estimator should satisfy two key properties: reliability, meaning that it provides an upper bound for the true error, and efficiency, meaning that it also reflects the error from below, at least up to multiplicative constants, oscillation terms (polynomial projection or stabilisation terms), and higher-order terms that vanish for very small mesh size ($h \rightarrow 0$). In the context of buckling eigenvalue problem a posteriori error estimation for FEM based discretisations of H^1 variational formulation have been proposed [22, 32] and adaptive based on FEM/VEM discretisations for H^2 variational formulation of the biharmonic problem can be found in [12, 16, 18, 25, 35].

Main contributions. To the best of the author’s knowledge, this work is the first that:

- Develop a reliable and efficient residual-based a posteriori error estimator for the C^1 -VEM applied to the buckling eigenvalue problem in both 2D and 3D.
- Account for nonlinear plane stress effects in the a posteriori error estimator, enabling accurate prediction of buckling modes in plates under complex multi-axial loading.
- Provide an open-source implementation within the `vem++` library [15], supporting computations on general polytopal meshes.

In Section 2, we introduce the H^2 variational formulation for the buckling eigenvalue problem and its spectral characterisation. Section 3 introduces the VEM space for both 2D and 3D together with a priori error estimates. The residual-based a posteriori error analysis is developed in Section 4. Finally, several numerical results illustrating the accuracy and applicability of the method are provided in Section 5.

Recurrent notation. This paper employs usual notation for differential operators in \mathbb{R}^d ($d = 2, 3$). In particular, the gradient, vector divergence, and tensor divergence operators are denoted by $\nabla : \mathbb{R} \rightarrow \mathbb{R}^d$, $\text{div} : \mathbb{R}^d \rightarrow \mathbb{R}$, and $\mathbf{div} : \mathbb{R}^{d \times d} \rightarrow \mathbb{R}^d$. The fourth-order biharmonic operator is denoted by $\Delta^2 : \mathbb{R} \rightarrow \mathbb{R}$, where $\Delta = \text{div}(\nabla)$. Finally, the Hessian matrix consists of all second-order partial derivatives and is denoted by $\nabla^2 : \mathbb{R} \rightarrow \mathbb{R}^{d \times d}$.

We adopt standard notation for Sobolev spaces, together with the associated norms and semi-norms (see e.g. [2]). By $a \lesssim b$ we denote the inequality $a \leq Cb$, where C is a generic positive constant independent of the mesh size h and can take different values on each occurrence.

2. The buckling eigenvalue problem

Let $\Omega \subseteq \mathbb{R}^d$ be a polytopal bounded domain with boundary $\Gamma := \partial\Omega$. The buckling mode $u : \Omega \rightarrow \mathbb{R}$, subjected to a plane stress tensor field $\boldsymbol{\kappa} : \Omega \rightarrow \mathbb{R}^{d \times d}$ with non-dimensional critical load factor $\lambda \in \mathbb{R}$ satisfy the following eigenvalue problem:

$$\Delta^2 u = -\lambda \text{div}(\boldsymbol{\kappa} \nabla u), \quad \text{in } \Omega, \quad (2.1a)$$

$$\mathcal{B}^j u = 0, \quad \text{on } \Gamma. \quad (2.1b)$$

Note that the non-dimensional critical load factor is normalised by multiplying by the factor L/D , where L denotes the plate size and $D = (Et^3)/(12(1 - \nu^2))$ is the bending stiffness, with E , t , and ν representing the Young's modulus, plate thickness, and Poisson's ratio. Whereas, the plane stress tensor is assumed to satisfy the following conditions

$$\boldsymbol{\kappa} \in [\mathbb{L}^\infty(\Omega)]^{d \times d} \setminus \{\mathbf{0}\}, \quad \boldsymbol{\kappa} = \boldsymbol{\kappa}^\top, \quad \mathbf{div}(\boldsymbol{\kappa}) = \mathbf{0}, \quad \text{in } \Omega.$$

The boundary conditions are defined through the linear differential operator \mathcal{B}^j (cf. (2.1b)) where $j \in \{\mathbf{SSP}, \mathbf{CP}\}$ (see e.g. [20, Section 2.3]). The notation **SSP** and **CP** indicate Simply Supported Plate and Clamped Plate type boundary conditions, defined respectively by

$$\mathcal{B}^{\mathbf{SSP}} u := \Delta^{\beta-1} u = 0, \quad \text{on } \Gamma, \quad (2.2a)$$

$$\mathcal{B}^{\mathbf{CP}} u := \partial_{\mathbf{n}}^{\beta-1} u = 0, \quad \text{on } \Gamma, \quad (2.2b)$$

where $\beta \in \{1, 2\}$, \mathbf{n} denotes be the outward unit normal vector to Γ , and $\partial_{\mathbf{n}}$ the normal derivative.

2.1. Weak formulation

In view of the boundary conditions (2.2a)-(2.2b), basic integration by parts lead to: find $(\lambda, u) \in \mathbb{R} \times (\mathbf{V} \setminus \{0\})$ such that

$$a(u, v) = \lambda b(u, v), \quad \forall v \in \mathbf{V}, \quad (2.3)$$

where the bilinear forms $a : \mathbf{V} \times \mathbf{V} \rightarrow \mathbb{R}$, $b : \mathbf{V} \times \mathbf{V} \rightarrow \mathbb{R}$ are defined by

$$a(u, v) := \int_{\Omega} \nabla^2 u : \nabla^2 v, \quad b(u, v) := \int_{\Omega} (\boldsymbol{\kappa} \nabla u) \cdot \nabla v.$$

Without losing generality, the space \mathbf{V} refers to $H^2(\Omega) \cap H_0^1(\Omega)$ and $H_0^2(\Omega)$ for the **SSP** and **CP** boundary conditions, respectively. It is well-known that standard arguments in Sobolev spaces imply the continuity of $a(\cdot, \cdot)$ and $b(\cdot, \cdot)$. Whereas, the generalised Poincaré inequality implies the ellipticity of $a(\cdot, \cdot)$ on \mathbf{V} . Thus, a straight-forward application of the Lax–Milgram Theorem proves the well-posedness of (2.3).

2.2. Spectral characterisation

It is well known that the spectrum of problem (2.3) can be characterised by the spectrum of a bounded, compact, and self-adjoint operator defined as follows (see, for instance, [13]):

$$\begin{aligned} T : V &\longrightarrow V \\ f &\longmapsto Tf, \end{aligned}$$

where, Tf is the unique solution of the following source problem:

$$a(Tf, v) = b(f, v), \quad \forall v \in V. \quad (2.4)$$

Moreover, the following result summarises some important properties of the operator T , we refer to [16, 28] for further details.

Theorem 2.1. *The following statements hold true*

- (i) *A pair (λ, u) solves (2.3) if and only if (μ, u) satisfies $Tu = \mu u$, for $\lambda \neq 0$ and $\mu := \lambda^{-1}$.*
- (ii) *The spectrum of T is given by $\text{sp}(T) = \{0\} \cup \{\mu_k\}_{k \in \mathbb{N}}$, where $\{\mu_k\}_{k \in \mathbb{N}} \subseteq \mathbb{R}$ is a sequence converging to zero, and each eigenvalue μ_k has finite multiplicity.*
- (iii) *If $\tilde{T} : H_0^1(\Omega) \longrightarrow V$ denotes the extension of T (cf. (2.4)) to $H_0^1(\Omega)$, then $\text{sp}(T) = \text{sp}(\tilde{T})$.*

3. A priori error analysis for the discrete spectral problem using virtual elements

In this section, we introduce the VEM spaces on polygonal/polyhedral meshes related to the discretisation of (2.1). First, we define the virtual spaces and projections over facets (which in 2D reduces to the local space over polygons). Then, the bulk spaces are defined and glued together to construct the global VEM space. We refer to [3, 6] for further details regarding the construction of the discrete spaces and well-posedness of the discrete problem.

Let Ω^h be a collection of polygonal/polyhedral meshes on Ω and \mathcal{F}^h be the set of all facets (edges in 2D and faces in 3D). The diameter of a polygon/polyhedron K is denoted by h_K and the diameter of a facet f is given by h_f . The maximum diameter of elements in Ω^h is represented by h . It is assumed that there exists a uniform constant $\rho > 0$ such that

- (M1) Every element K is star-shaped with respect to a ball with a radius greater than ρh_K .
- (M2) Every facet $f \in \partial K$ is star-shaped with respect to a ball with a radius greater than ρh_K .
- (M3) Every facet $f \in \partial K$ satisfies the inequality $h_f \geq \rho h_K$.

We split the set of all facets as $\mathcal{F}^h = \mathcal{F}_\Omega^h \cup \mathcal{F}_\Gamma^h$, where $\mathcal{F}_\Omega^h = \{f \in \mathcal{F}^h : f \subset \Omega\}$, $\mathcal{F}_\Gamma^h = \{f \in \mathcal{F}^h : f \subset \Gamma\}$. The set of facets of $K \in \Omega^h$ is denoted as $\mathcal{F}^h(K)$, who in turn are classified as interior and boundary facets, denoted by $\mathcal{F}_\Omega^h(K)$ and $\mathcal{F}_\Gamma^h(K)$, respectively. The set of elements K that share f as a facet is denoted by Ω_f^h and the normal jump operator is defined as usual by $\llbracket \nabla u \cdot \mathbf{n}_f \rrbracket := (\nabla u|_K - \nabla u|_{K'})|_f \cdot \mathbf{n}_f$, where $K, K' \in \Omega_f^h$, and \mathbf{n}_f is the outward normal vectors of f with respect to ∂K . In addition, we denote by \mathcal{V}_Γ^h and \mathcal{V}_Ω^h the sets of boundary and interior vertices in $\overline{\Omega^h}$, respectively. On the other hand, Δ_f and ∇_f denote the respective Laplace and gradient operators in the local facet coordinates and $\partial_{\mathbf{n}_f^e}$ denotes the normal derivative on each ridge $e \in \partial f$ with respect to f (similarly for $\partial_{\mathbf{n}_K^f}$).

3.1. Polynomial Projection operators

The space of polynomials of total degree at most k defined locally on $K \in \Omega^h$ (or facet $f \in \mathcal{F}^h$) is denoted by $\mathbf{P}_k(K)$, and its vector counterparts is denoted by $\mathbf{P}_k(K)$. We also consider the standard notation $\mathbf{P}_{-1}(K) = \{0\}$. In this paper, we consider the lowest-case order VEM discretisation where $k = 2$. Then, we define local polynomial projection operators in an element $K \in \Omega^h$, as follows:

- The vector \mathbf{L}^2 projection $\mathbf{\Pi}_K^0 : \mathbf{L}^2(K) \rightarrow \mathbf{P}_1(K)$ with

$$\int_K (\mathbf{v} - \mathbf{\Pi}_K^0 \mathbf{v}) \cdot \mathbf{p}_1 = 0, \quad \forall \mathbf{p}_1 \in \mathbf{P}_1(K). \quad (3.1)$$

- The \mathbf{H}^1 -energy projection $\mathbf{\Pi}_K^\nabla : \mathbf{H}^1(K) \rightarrow \mathbf{P}_2(K)$ is defined as

$$\begin{aligned} \int_K \nabla(\mathbf{\Pi}_K^\nabla v_h - v_h) \cdot \nabla p_2 &= 0, \quad \forall p_2 \in \mathbf{P}_2(K), \\ \int_{\partial K} (\mathbf{\Pi}_K^\nabla v_h - v_h) &= 0. \end{aligned}$$

- The \mathbf{H}^2 -energy projection is defined as $\mathbf{\Pi}_K^{\nabla^2} : \mathbf{H}^2(K) \rightarrow \mathbf{P}_2(K)$ such that

$$\begin{aligned} \int_K \nabla^2(\mathbf{\Pi}_K^{\nabla^2} v_h - v_h) : \nabla^2 p_2 &= 0, \quad \forall p_2 \in \mathbf{P}_2(K), \\ \int_{\partial K} (\mathbf{\Pi}_K^{\nabla^2} v_h - v_h) p_1 &= 0, \quad \forall p_1 \in \mathbf{P}_1(f). \end{aligned}$$

Notice that, the previous definitions are also valid for facets $f \in \mathcal{F}^h$, in this case we simply write $\mathbf{\Pi}_f^\nabla$ and $\mathbf{\Pi}_f^{\nabla^2}$. Moreover, the projections operators previously defined are computable directly from the degrees of freedom of the VEM discrete spaces (to be specified in Section 3.2), we refer to [3, 6] for further details.

We finalise by stating a result involving classical polynomial approximation theory, written for a general polynomial order of approximation in the elements $K \in \Omega^h$. Recall that similar estimates can be deduced for facets $f \in \mathcal{F}^h$ and vector valued functions (see e.g. [8]).

Proposition 3.1 (polynomial approximation). *Given $K \in \Omega^h$, suppose that $v \in \mathbf{H}^s(K)$, with $1 \leq s \leq k + 1$. Then, there exist $v_\pi \in \mathbf{P}_k(K)$ and a positive constant that depends only on ρ (cf. **(M1)**-**(M3)**) such that for $0 \leq r \leq s$ the following estimate holds*

$$|v - v_\pi|_{r,K} \lesssim h_K^{s-r} |v|_{s,K}.$$

3.2. Discrete spaces

We start by considering the enhanced space on facets $f \in \partial K$ (see [3]), given by

$$\begin{aligned} \mathbf{V}_{2D}^h(f) &:= \left\{ v_h \in \mathbf{H}^2(f) : \Delta_f^2 v_h \in \mathbf{P}_2(f), \right. \\ &\quad v_h|_{\partial f} \in C^0(\partial f), v_h|_e \in \mathbf{P}_3(e), \quad \forall e \in \partial f, \\ &\quad \nabla_f v_h|_{\partial f} \in [C^0(\partial f)]^2, \partial_{\mathbf{n}_f^\varepsilon} v_h|_e \in \mathbf{P}_1(e), \quad \forall e \in \partial f, \end{aligned}$$

$$\int_f \Pi_f^{\nabla^2} v_h p_2 = \int_f v_h p_2, \quad \forall p_2 \in P_2(f).$$

Notice that in a 2D setting, one can identify the facets f and ridge $e \in \partial f$ in the previous space as polygonal elements K and edges of the polygon e , respectively. Such identifications allow us to define directly the global 2D VEM space by

$$V_{2D}^h := \{v_h \in V : v_h|_K \in V_{2D}^h(K)\}.$$

We remark that the space $V_{2D}^h(f)$ is richer to its 3D counterpart introduced in [6], where the condition $\Delta_f^2 v_h \in P_1(f)$ is imposed and the enhancement property is enforced only with respect to linear polynomials.

Next, following the hierarchical construction of VEM spaces in 3D, we introduce an additional enhanced space on facets in order to represent normal derivatives of virtual functions in facets, as follows

$$\begin{aligned} V_{\partial}^h(f) := & \left\{ v_h \in H^1(f) : \Delta_f v_h \in P_0(f), \right. \\ & v_h|_{\partial f} \in C^0(\partial f), v_h|_e \in \mathbb{P}_1(e), \quad \forall e \in \partial f, \\ & \left. \int_f \Pi_f^{\nabla} v_h = \int_f v_h \right\}. \end{aligned}$$

With these building blocks, we are ready to define the local three-dimensional VEM space on a polyhedron $K \in \Omega^h$ as

$$\begin{aligned} V_{3D}^h(K) := & \left\{ v_h \in H^2(K) : \Delta^2 v_h \in P_2(K), \right. \\ & v_h|_e \in C^0(e), \nabla v_h|_e \in [C^0(e)]^3, \quad \forall e \in \bigcup_{f \in \partial K} \partial f, \\ & v_h|_f \in V_{2D}^h(f), \partial_{\mathbf{n}_K} v_h|_f \in V_{\partial}^h(f), \quad \forall f \in \partial K, \\ & \left. \int_K \Pi_K^{\nabla^2} v_h p_2 = \int_K v_h p_2, \quad \forall p_2 \in P_2(K) \right\}, \end{aligned}$$

Similarly, the global space is obtained by gluing together the local spaces in the following way

$$V_{3D}^h := \{v_h \in V : v_h|_K \in V_{3D}^h(K)\}.$$

Following [3, 6], a unisolvent set of degrees of freedom for $V^h(K)$ can be chosen as

- The values of v_h at the vertices of K ,
- The values of ∇v_h at the vertices of K .

Thanks to this selection, we have that

$$\dim(V_{2D}^h) = \begin{cases} 3\#(\mathcal{V}_{\Omega^o}^h) & \text{for } \mathbf{CP}, \\ 3\#(\mathcal{V}_{\Omega^o}^h) - 2\#(\mathcal{V}_{\Gamma}^h) & \text{for } \mathbf{SSP}. \end{cases}$$

and

$$\dim(\mathbf{V}_{3\text{D}}^h) = \begin{cases} 4\#(\mathcal{V}_{\Omega^o}^h) & \text{for } \mathbf{CP}, \\ 4\#(\mathcal{V}_{\Omega^o}^h) - 3\#(\mathcal{V}_{\Gamma}^h) & \text{for } \mathbf{SSP}. \end{cases}$$

Finally, we introduce the notation $\mathbf{V}_h(K)$ (resp. \mathbf{V}_h) to denote simultaneously the local spaces $\mathbf{V}_{2\text{D}}^h(K)$ and $\mathbf{V}_{3\text{D}}^h(K)$ (resp. global spaces $\mathbf{V}_{3\text{D}}^h$ and $\mathbf{V}_{2\text{D}}^h$). Furthermore, the previous hierarchical construction is C^1 continuous along the elements' facets, which turns into discrete functions that are C^1 continuous globally.

3.3. Discrete weak formulation

We start by defining locally the computable discrete bilinear forms for all $u_h, v_h \in \mathbf{V}_h$ as follows

$$\begin{aligned} a_K^h(u_h, v_h) &:= \int_K \nabla^2(\Pi_K^{\nabla^2} u_h) : \nabla^2(\Pi_K^{\nabla^2} v_h) + S_K^{\nabla^2}(u_h - \Pi_K^{\nabla^2} u_h, v_h - \Pi_K^{\nabla^2} v_h), \\ b_K^h(u_h, v_h) &:= \int_K (\boldsymbol{\kappa} \Pi_K^0(\nabla u_h)) \cdot \Pi_K^0(\nabla v_h), \end{aligned}$$

where the operator $S_K^{\nabla^2} : \mathbf{V} \times \mathbf{V} \rightarrow \mathbb{R}$ is any symmetric positive bilinear form that satisfies

$$\alpha_* a_K(v_h, v_h) \leq S_K^{\nabla^2}(v_h, v_h) \leq \alpha^* a_K(v_h, v_h), \quad \forall v_h \in \ker(\Pi_K^{\nabla^2}), \quad (3.4)$$

here, α_*, α^* are positive constants independent of the element size h_K . Notice that the properties of the stabilization operator are given in (3.4) is crucial to prove the continuity and ellipticity of $a^h(\cdot, \cdot)$, $b^h(\cdot, \cdot)$ (defined as the sum of the local contributions for all $K \in \Omega^h$) and ellipticity of $a^h(\cdot, \cdot)$, we refer to [17, 29] for further details.

Now we are ready to introduce the VEM discrete weak formulation of (2.1) read as follows: find $(\lambda_h, u_h) \in \mathbb{R} \times (\mathbf{V}_h \setminus \{0\})$ such that

$$a^h(u_h, v_h) = \lambda_h b^h(u_h, v_h), \quad \forall v_h \in \mathbf{V}_h. \quad (3.5)$$

3.4. The a priori error analysis

We start recalling the orthogonal projection $\mathcal{P}_h^\nabla : H_0^1(\Omega) \rightarrow V_h$ defined as follows: For all $\phi \in H_0^1(\Omega)$ we set $\mathcal{P}_h^\nabla \phi \in V_h$ as unique solution of

$$\int_{\Omega} \nabla(\mathcal{P}_h^\nabla \phi - \phi) \cdot \nabla v_h, \quad \forall v_h \in V_h.$$

Remark 3.1. If $\boldsymbol{\kappa}$ additionally satisfies the positive definiteness assumption, then the operator $\mathcal{P}_h^\nabla : H_0^1(\Omega) \rightarrow V_h$ given by

$$b(\mathcal{P}_h^\nabla \phi - \phi, v_h) = 0, \quad \forall v_h \in V_h,$$

is well defined.

Next, we consider the discrete source operators

$$\begin{aligned} T_h : V_h &\longrightarrow V_h & \text{and} & & \widehat{T}_h : H_0^1(\Omega) &\longrightarrow V_h \subset H_0^1(\Omega) \\ f_h &\longmapsto T_h f_h & & & f &\longmapsto \widehat{T}_h f := T_h \mathcal{P}_h^\nabla f \end{aligned}$$

where $T_h f_h$ and $T_h \mathcal{P}_h^\nabla f$ are the unique solutions of the following discrete source problems

$$a^h(T_h f_h, v_h) = b^h(f_h, v_h) \quad \text{and} \quad a^h(T_h \mathcal{P}_h^\nabla f, v_h) = b^h(\mathcal{P}_h^\nabla f, v_h), \quad (3.6)$$

for all $v_h \in V_h$, respectively. It is well known that the operators \widehat{T}_h and T_h satisfy $\text{sp}(\widehat{T}_h) = \text{sp}(T_h)$ and they have the same eigenfunctions (see for instance [17]). In addition, if $Z_h := \{u_h \in V_h : b^h(u_h, v_h) = 0 \quad \forall v_h \in V_h\}$, we readily see that the spectrum $\text{sp}(T_h)$ consists of $\dim(V_h) - \dim(Z_h) =: M$ eigenvalues repeated according to their respective multiplicity. Moreover, it holds that $\text{sp}(T_h) = \{\mu_h\}_{k=1}^M \cup \{0\}$.

On the other hand, for (T, μ) and (T_h, μ_h) , we recall the definitions of their spectral projections E and E_h as

$$\begin{aligned} E &:= E(\mu) = (2\pi)^{-1} \int_{\Omega} (z - T)^{-1} dz, \\ E_h &:= E_h(\mu) = (2\pi)^{-1} \int_{\Omega} (z - T_h)^{-1} dz, \end{aligned} \quad (3.7)$$

where $\mu_h := 1/\lambda_h$, ($\lambda_h \neq 0$). Finally, we establish error estimates for the solution of the source problems in H^2 and H^1 norms (see for instance [16] and [29]).

Lemma 3.1. *For $s \in (1/2, 1]$ it holds*

$$\begin{aligned} \|(T - \widehat{T}_h)(f)\|_{2,\Omega} &\lesssim h^s \|f\|_{2,\Omega}, \quad \forall f \in V, \\ \|(\widetilde{T} - \widehat{T}_h)(f)\|_{1,\Omega} &\lesssim h^s \|f\|_{1,\Omega}, \quad \forall f \in H_0^1(\Omega). \end{aligned}$$

We now prove an useful relation between the continuous and discrete bilinear forms $b(\cdot, \cdot)$ and $b^h(\cdot, \cdot)$.

Lemma 3.2. *For all $v_h, w_h \in V_h$ it holds*

$$b(v_h, w_h) - b^h(v_h, w_h) = \sum_{K \in \Omega^h} \int_K \left(\kappa \nabla v_h - \mathbf{\Pi}_K^0(\kappa \nabla v_h) \right) \cdot \left(\nabla w_h - \mathbf{\Pi}_K^0 \nabla w_h \right)$$

Proof. Let $v_h, w_h \in V_h$ and $K \in \Omega^h$. From the definition of the projector $\mathbf{\Pi}_K^0$ (cf. (3.1)) and some algebraic manipulations, we readily see that

$$\begin{aligned} b_K(v_h, w_h) - b_K^h(v_h, w_h) &= \int_K \left\{ \kappa \nabla v_h \cdot \nabla w_h - \kappa \mathbf{\Pi}_K^0 \nabla v_h \cdot \mathbf{\Pi}_K^0 \nabla w_h \right\} \\ &= \int_K \left\{ \kappa \nabla v_h \cdot \nabla w_h - \mathbf{\Pi}_K^0(\kappa \mathbf{\Pi}_K^0 \nabla v_h) \cdot \mathbf{\Pi}_K^0 \nabla w_h \right\} \\ &= \int_K \left\{ [\kappa \nabla v_h - \mathbf{\Pi}_K^0(\kappa \nabla v_h)] \cdot \nabla w_h + \mathbf{\Pi}_K^0(\kappa \nabla v_h) \cdot [\nabla w_h - \mathbf{\Pi}_K^0 \nabla w_h] \right. \\ &\quad + \mathbf{\Pi}_K^0 \nabla w_h \cdot [\mathbf{\Pi}_K^0(\kappa \nabla v_h) - \kappa \nabla v_h] + \mathbf{\Pi}_K^0 \nabla w_h \cdot \kappa [\nabla v_h - \mathbf{\Pi}_K^0 \nabla v_h] \\ &\quad \left. + \mathbf{\Pi}_K^0 \nabla w_h \cdot [\kappa \mathbf{\Pi}_K^0 \nabla v_h - \mathbf{\Pi}_K^0(\kappa \mathbf{\Pi}_K^0 \nabla v_h)] \right\} \\ &= \int_K [\kappa \nabla v_h - \mathbf{\Pi}_K^0(\kappa \nabla v_h)] \cdot \nabla w_h \end{aligned}$$

$$= \int_K [\boldsymbol{\kappa} \nabla v_h - \mathbf{\Pi}_K^0(\boldsymbol{\kappa} \nabla u_h)] \cdot [\nabla w_h - \mathbf{\Pi}_K^0 \nabla w_h].$$

By taking sum over all $K \in \Omega^h$, the result is obtained. \square

We now introduce an error estimate for λ_h as a consequence of Lemmas 3.1 and 3.2.

Theorem 3.1. *For all space $R(E) \subseteq H^{2+s}(\Omega)$ with $s \in (1/2, 1]$ there exists $h_0 > 0$ independent of h such that for all $h < h_0$ it hold*

$$\begin{aligned} |\lambda - \lambda_h^{(j)}| &\lesssim h^{2s}, \quad j = 1, \dots, m, \quad \text{and} \\ |\lambda - \lambda_h^{(j)}| &\lesssim \left\{ |u - u_h|_{2,\Omega}^2 + |u - \mathbf{\Pi}_K^{\nabla^2} u_h|_{2,h}^2 + \|\boldsymbol{\kappa} \nabla u_h - \mathbf{\Pi}_K^0(\boldsymbol{\kappa} \nabla u)\|_{0,\Omega} \|\nabla u_h - \mathbf{\Pi}_K^0(\nabla u_h)\|_{0,\Omega} \right\}. \end{aligned}$$

Proof. The first inequality follows as a direct consequence of Lemma 3.1. Regarding the second inequality, following the arguments used in the proof of the [28, Theorem 4.4] and applying Lemma 3.2, we readily see that

$$\begin{aligned} (\lambda_h^{(j)} - \lambda) b^h(u_h, u_h) &= a(u - u_h, u - u_h) - \lambda b(u - u_h, u - u_h) + \{a^h(u_h, u_h) - a(u_h, u_h)\} \\ &\quad + \lambda \{b(u_h, u_h) - b^h(u_h, u_h)\} \\ &\lesssim |u - u_h|_{2,\Omega}^2 + \|\mathbf{\Pi}_K^0 \nabla(u - u_h)\|_{0,\Omega}^2 + |u - u_h|_{2,\Omega}^2 + |u - \mathbf{\Pi}_K^{\nabla^2} u_h|_{2,h}^2 \\ &\quad + \|\boldsymbol{\kappa} \nabla u_h - \mathbf{\Pi}_K^0(\boldsymbol{\kappa} \nabla u)\|_{0,\Omega} \|\nabla u_h - \mathbf{\Pi}_K^0(\nabla u_h)\|_{0,\Omega} \\ &\lesssim |u - u_h|_{2,\Omega}^2 + |u - \mathbf{\Pi}_K^{\nabla^2} u_h|_{2,h}^2 \\ &\quad + \|\boldsymbol{\kappa} \nabla u_h - \mathbf{\Pi}_K^0(\boldsymbol{\kappa} \nabla u)\|_{0,\Omega} \|\nabla u_h - \mathbf{\Pi}_K^0(\nabla u_h)\|_{0,\Omega}, \end{aligned}$$

where, in the last step we have used the boundedness of $\mathbf{\Pi}_K^0$ and Poincaré inequality (cf. $u - u_h \in V$). Moreover, the ellipticity of $a^h(\cdot, \cdot)$ implies that

$$|b^h(u_h, u_h)| = |\lambda_h^{-1} a^h(u_h, u_h)| \gtrsim |\lambda_h^{-1}| > 0,$$

and the result follows. \square

An error estimate for the solutions of the source problems (2.4) and (3.6) is given below.

Lemma 3.3. *Given any $f \in R(E)$ set $w := Tf$ and $w_h := \widehat{T}_h f$, then, the following estimate holds*

$$\begin{aligned} |w - w_h|_{2,\Omega} &\lesssim h^s \left\{ |w - w_h|_{2,\Omega} + |w - \mathbf{\Pi}^{\nabla^2} w_h|_{2,h} \right\} \\ &\quad + h^{1+s} \|\boldsymbol{\kappa} \nabla w - \mathbf{\Pi}_K^0(\boldsymbol{\kappa} \nabla w)\|_{0,\Omega} v + |w - \mathcal{P}_h^\nabla w|_{1,\Omega}, \end{aligned}$$

where $R(E)$ denotes the range of the operator E (cf. (3.7)).

Proof. Given $f \in R(E)$, set $w := Tf$ and $w_h := \widehat{T}_h f$ as the solutions of problems (2.4) and (3.6) (respectively), let $v \in V$ the unique solution of the following weak variational formulation: find $v \in V$, such that

$$a(v, z) = \int_\Omega \nabla(w - w_h) \cdot \nabla z \quad \forall z \in V. \quad (3.8)$$

It is easy to check that $T(w - w_h) = v$ (cf. (2.4)), and the Lax-Milgram Theorem implies $|v|_{2,\Omega} \lesssim \|\kappa\|_{\infty,\Omega} |w - w_h|_{1,\Omega}$. In addition, since $v \in H^{2+s}(\Omega)$, we have that there exists $v_I \in V_h$ such $|v - v_I|_{2,\Omega} \lesssim h^s |v|_{2+s,\Omega}$ (cf. [21]). Then, testing (3.8) with $w - w_h \in V$, we get

$$\begin{aligned} |w - w_h|_{1,\Omega}^2 &= \int_{\Omega} \nabla(w - w_h) \cdot \nabla(w - w_h) \\ &= a(v - v_I, w - w_h) + a(v_I, w - w_h) \\ &= a(v - v_I, w - w_h) + a(w, v_I) - a(w_h, v_I) + a^h(w_h, v_I) - a^h(w_h, v_I) \\ &= a(v - v_I, w - w_h) + \{a^h(w_h, v_I) - a(w_h, v_I)\} + \{b(f, v_I) - b^h(\mathcal{P}_h^\nabla f, v_I)\}. \end{aligned}$$

From [16, Lemma 10], we have that

$$|w - w_h|_{1,\Omega}^2 \leq h^s \left\{ |w - w_h|_{2,\Omega} + |w - \Pi^{\nabla^2} w_h|_{2,h} \right\} |w - w_h|_{1,\Omega} + \{b(f, v_I) - b^h(\mathcal{P}_h^\nabla f, v_I)\}. \quad (3.9)$$

Now, by adding and subtracting the term $b(\mathcal{P}_h^\nabla f, v_I)$, applying Lemma 3.2 and $f = \mu^{-1}w$ in the last term of (3.9), we arrive at

$$\begin{aligned} b(f, v_I) - b^h(\mathcal{P}_h^\nabla f, v_I) &= b(f - \mathcal{P}_h^\nabla f, v_I) + \{b(\mathcal{P}_h^\nabla f, v_I) - b^h(\mathcal{P}_h^\nabla f, v_I)\} \\ &= b(f - \mathcal{P}_h^\nabla f, v_I) \\ &\quad + \sum_{K \in \Omega^h} \int_K [\kappa \nabla(\mathcal{P}_h f) - \mathbf{\Pi}_K^0(\kappa \nabla(\mathcal{P}_h f))] \cdot [\nabla v_I - \mathbf{\Pi}_K^0(\nabla v_I)] \\ &= \mu^{-1} \left\{ b(w - \mathcal{P}_h^\nabla w, v_I) \right. \\ &\quad \left. + \sum_{K \in \Omega^h} \int_K [\kappa \nabla(\mathcal{P}_h^\nabla w) - \mathbf{\Pi}_K^0(\kappa \nabla(\mathcal{P}_h^\nabla w))] \cdot [\nabla v_I - \mathbf{\Pi}_K^0(\nabla v_I)] \right\}. \quad (3.10) \end{aligned}$$

Next, by adding and subtracting the terms ∇v and $\mathbf{\Pi}_K^0 \nabla v$, applying the Cauchy-Schwarz inequality and the additional regularity of v in (3.10), we obtain

$$b(f, v_I) - b^h(\mathcal{P}_h^\nabla f, v_I) \lesssim |b(w - \mathcal{P}_h^\nabla w, v_I)| + h^{1+s} \|\kappa \nabla(\mathcal{P}_h w) - \mathbf{\Pi}_K^0(\kappa \nabla(\mathcal{P}_h w))\|_{0,\Omega} |w - w_h|_{1,\Omega}.$$

Note that the addition and subtraction of the terms $\kappa \nabla w$ and $\mathbf{\Pi}_K^0(\kappa \nabla w)$ together with the triangle inequality, the assumption $\kappa \in L^\infty(\Omega)$ and the fact that $|w - \mathcal{P}_h w|_{1,\Omega} = \inf_{z_h \in V_h} |w - z_h|_{1,\Omega}$ applied to the last term of the above expression, we obtain

$$\begin{aligned} b(f, v_I) - b^h(\mathcal{P}_h^\nabla f, v_I) &\lesssim |b(w - \mathcal{P}_h^\nabla w, v_I)| + h^{1+s} \left\{ |\mathcal{P}_h^\nabla w - w|_{1,\Omega} \right. \\ &\quad \left. + \|\kappa \nabla w - \mathbf{\Pi}_K^0(\kappa \nabla w)\|_{0,\Omega} + |w - \mathcal{P}_h^\nabla w|_{1,\Omega} \right\} |w - w_h|_{1,\Omega} \\ &\lesssim |b(w - \mathcal{P}_h^\nabla w, v_I)| \\ &\quad + h^{1+s} \left\{ |w - w_h|_{1,\Omega} + \|\kappa \nabla w - \mathbf{\Pi}_K^0(\kappa \nabla w)\|_{0,\Omega} \right\} |w - w_h|_{1,\Omega}. \quad (3.11) \end{aligned}$$

Finally, by inserting the estimate (3.11) in the right-hand side of (3.9) and multiplying by $|w - w_h|_{1,\Omega}^{-1}$ in (3.9) we have

$$\begin{aligned}
|w - w_h|_{2,\Omega} &\lesssim h^s \left\{ |w - w_h|_{2,\Omega} + |w - \Pi^{\nabla^2} w_h|_{2,h} \right\} \\
&\quad + h^{1+s} \left\{ |w - w_h|_{1,\Omega} + \|\kappa \nabla w - \Pi_K^0(\kappa \nabla w)\|_{0,\Omega} \right\} + |b(w - \mathcal{P}_h^\nabla w, v_I)| \\
&\lesssim h^s \left\{ |w - w_h|_{2,\Omega} + |w - \Pi^{\nabla^2} w_h|_{2,h} \right\} \\
&\quad + h^{1+s} \|\kappa \nabla w - \Pi_K^0(\kappa \nabla w)\|_{0,\Omega} v + |b(w - \mathcal{P}_h^\nabla w, v_I)| \\
&\lesssim h^s \left\{ |w - w_h|_{2,\Omega} + |w - \Pi^{\nabla^2} w_h|_{2,h} \right\} \\
&\quad + h^{1+s} \|\kappa \nabla w - \Pi_K^0(\kappa \nabla w)\|_{0,\Omega} v + |w - \mathcal{P}_h^\nabla w|_{1,\Omega}.
\end{aligned}$$

□

As a consequence of the previous result, we have

Corollary 3.1. *If the assumption in Remark 3.1 is satisfied, then*

$$|w - w_h|_{2,\Omega} \lesssim h^s \left\{ |w - w_h|_{2,\Omega} + |w - \Pi^{\nabla^2} w_h|_{2,h} \right\} + h^{1+s} \|\kappa \nabla w - \Pi_K^0(\kappa \nabla w)\|_{0,\Omega},$$

for all $f \in R(E) \subset H^{2+s}(\Omega)$ such that $w := Tf$ and $w_h := \widehat{T}_h f$.

We finalise by introducing an error estimate in the H^1 semi-norm for the spectral problem (3.5).

Lemma 3.4. *For all eigenpairs $(\mu_h^{(j)}, u_h)$ of \widehat{T}_h such that $\|u_h\|_{1,\Omega} = 1$ ($j = 1, 2, \dots, m$), there exists an eigenfunction $u \in H_0^1(\Omega)$ of T associated with μ such that*

$$|u - u_h|_{1,\Omega} \lesssim h^s \left\{ |w - w_h|_{2,\Omega} + |w - \Pi_K^{\nabla^2} w_h|_{2,h} \right\} + h^{1+s} \|\kappa \nabla w - \Pi_K^0(\kappa \nabla w)\|_{0,\Omega} + |w - \mathcal{P}_h^\nabla w|_{1,\Omega}.$$

Proof. The proof follows with the same arguments presented in [16, Lemma 11]. □

Theorem 3.2. *If u and u_h solve the continuous and discrete spectral problems (2.3) and (3.5), respectively. Then, there exists $s \in (1/2, 1]$ such that*

$$|u - u_h|_{1,\Omega} \lesssim h^s \left\{ |u - u_h|_{2,\Omega} + |u - \Pi_K^{\nabla^2} u_h|_{2,h} \right\} + h^{1+s} \|\kappa \nabla u - \Pi_K^0(\kappa \nabla u)\|_{0,\Omega} + |u - \mathcal{P}_h^\nabla u|_{1,\Omega}.$$

Proof. The proof can be obtained from Lemma 3.4 with the same arguments as used in the proof of [16, Theorem 12] and

$$\|\kappa \nabla w - \Pi_K^0(\kappa \nabla w)\|_{0,\Omega} \lesssim |\mu^{-1}| \|\kappa \nabla u - \Pi_K^0(\kappa \nabla u)\|_{0,\Omega}.$$

□

4. Residual-based a posteriori error analysis

This section aims to define a residual-type estimator based on computable quantities of the VEM solution. In addition, we establish the reliability and efficiency of the proposed estimator. The upper bound follows from the residual equation combined with polynomial projections, stabilization terms, and interpolation estimates, while the lower bound is guaranteed through properties of bubble functions.

4.1. Error estimators

For each $K \in \Omega^h$ and $f \in \partial K$, the local estimators corresponding to the volume residual, the jump residual, the data oscillation, and the stabilisation term are defined by

$$\Xi_K^2 := h_K^4 \|\lambda_h \operatorname{div}(\mathbf{\Pi}_K^0(\boldsymbol{\kappa}\mathbf{\Pi}_K^0(\nabla u_h)))\|_{0,K}^2, \quad (4.1a)$$

$$\mathcal{J}_f^2 := h_f \|\llbracket (\nabla^2 \mathbf{\Pi}_K^{\nabla^2} u_h) \mathbf{n}_K^f \rrbracket\|_{0,f}^2 + h_f^3 \|\llbracket \lambda_h \mathbf{\Pi}_K^0(\boldsymbol{\kappa}\mathbf{\Pi}_K^0(\nabla u_h)) \cdot \mathbf{n}_K^f \rrbracket\|_{0,f}^2, \quad (4.1b)$$

$$\Lambda_K^2 := h_K^2 \|\lambda_h (\boldsymbol{\kappa}\mathbf{\Pi}_K^0(\nabla u_h) - \mathbf{\Pi}_K^0(\boldsymbol{\kappa}\mathbf{\Pi}_K^0(\nabla u_h)))\|_{0,K}^2, \quad (4.1c)$$

$$S_K^2 := S_K^{\nabla^2}(u_h - \mathbf{\Pi}_K^{\nabla^2} u_h, u_h - \mathbf{\Pi}_K^{\nabla^2} u_h). \quad (4.1d)$$

Notice that, the volume residual $\Xi^2 := \sum_{K \in \Omega^h} \Xi_K^2$ contains a polynomial approximation of the right-hand related to the buckling eigenvalue problem (cf. (2.1a)); recovering the full residual requires the use of higher-order approximations. In addition, the jump residual $\mathcal{J}^2 := \sum_{f \in \mathcal{F}_\Omega^h} \mathcal{J}_f^2$, and the stabilisation term $S^2 := \sum_{K \in \Omega^h} S_K^2$ are composed by computable polynomial projections of the discrete solution u_h . On the other hand, the data oscillation $\Lambda^2 := \sum_{K \in \Omega^h} \Lambda_K^2$ measures the polynomial approximation error of $\boldsymbol{\kappa}\nabla\mathbf{\Pi}_K^{\nabla^2} u_h$. Finally, the respective global total error estimator is defined as follows:

$$\eta^2 := \sum_{K \in \Omega^h} \eta_K^2 = \sum_{K \in \Omega^h} [\Xi_K^2 + \Lambda_K^2 + S_K^2] + \sum_{f \in \mathcal{F}_\Omega^h} \mathcal{J}_f^2 = \Xi^2 + \mathcal{J}^2 + \Lambda^2 + S^2.$$

4.2. Reliability

This section aims to prove an upper bound of the error in terms of the a posteriori error estimator. We start by rewriting the term $a(u - u_h, v)$ in terms of residual equations, from which the local error estimators emerge in a natural way during the subsequent analysis.

Lemma 4.1. *If u and u_h solve the spectral problems (2.3) and (3.5), then for every $v \in V$, the following identity holds:*

$$\begin{aligned} a(u - u_h, v) &= \lambda b(u, v) - \lambda_h b(u_h, v) + \sum_{K \in \Omega^h} a_K(\mathbf{\Pi}_K^{\nabla^2} u_h - u_h, v) \\ &\quad + \lambda_h \sum_{K \in \Omega^h} \int_K (\boldsymbol{\kappa}(\nabla u_h - \mathbf{\Pi}_K^0(\nabla u_h))) \cdot \nabla v - \sum_{K \in \Omega^h} \int_K \lambda_h \operatorname{div}(\mathbf{\Pi}_K^0(\boldsymbol{\kappa}\mathbf{\Pi}_K^0(\nabla u_h))) v \\ &\quad - \sum_{f \in \mathcal{F}_\Omega^h} \int_f \llbracket (\nabla^2 \mathbf{\Pi}_K^{\nabla^2} u_h) \mathbf{n}_K^f \rrbracket \cdot \nabla v + \sum_{f \in \mathcal{F}_\Omega^h} \int_f \llbracket \lambda_h \mathbf{\Pi}_K^0(\boldsymbol{\kappa}\mathbf{\Pi}_K^0(\nabla u_h)) \cdot \mathbf{n}_K^f \rrbracket v \\ &\quad + \sum_{K \in \Omega^h} \int_K \lambda_h (\boldsymbol{\kappa}\mathbf{\Pi}_K^0(\nabla u_h) - \mathbf{\Pi}_K^0(\boldsymbol{\kappa}\mathbf{\Pi}_K^0(\nabla u_h))) \cdot \nabla v. \end{aligned}$$

Proof. Fix $v \in V$. Since (λ, u) solves the weak buckling eigenvalue problem (cf. (2.3)), basic algebraic manipulations lead to

$$\begin{aligned} a(u - u_h, v) &= \lambda b(u, v) - \lambda_h b(u_h, v) + \lambda_h b(u_h, v) - a(u_h, v) \\ &= \lambda b(u, v) - \lambda_h b(u_h, v) + \sum_{K \in \Omega^h} \left[-a_K(u_h - \mathbf{\Pi}_K^{\nabla^2} u_h, v) - a_K(\mathbf{\Pi}_K^{\nabla^2} u_h, v) \right] \end{aligned}$$

$$\begin{aligned}
& + \lambda_h \sum_{K \in \Omega^h} \int_K (\boldsymbol{\kappa}(\nabla u_h - \boldsymbol{\Pi}_K^0(\nabla u_h)) \cdot \nabla v + \lambda_h \int_K \boldsymbol{\Pi}_K^0(\boldsymbol{\kappa} \boldsymbol{\Pi}_K^0(\nabla u_h)) \cdot \nabla v \\
& + \lambda_h \int_K [\boldsymbol{\kappa} \boldsymbol{\Pi}_K^0(\nabla u_h) - \boldsymbol{\Pi}_K^0(\boldsymbol{\kappa} \boldsymbol{\Pi}_K^0(\nabla u_h))] \cdot \nabla v. \tag{4.2}
\end{aligned}$$

Next, integration by parts and using that $\boldsymbol{\Pi}_K^{\nabla^2} u_h \in \mathbb{P}_2(K)$ imply that

$$\sum_{K \in \Omega^h} a_K(\boldsymbol{\Pi}_K^{\nabla^2} u_h, v) = \sum_{K \in \Omega^h} \int_{\partial K} \left(\nabla^2(\boldsymbol{\Pi}_K^{\nabla^2} u_h) \mathbf{n}_K \right) \cdot \nabla v. \tag{4.3}$$

Whereas, integration by parts lead to

$$\begin{aligned}
\sum_{K \in \Omega^h} \int_K \boldsymbol{\Pi}_K^0(\boldsymbol{\kappa} \boldsymbol{\Pi}_K^0(\nabla u_h)) \cdot \nabla v & = - \sum_{K \in \Omega^h} \int_K \operatorname{div} \left(\boldsymbol{\Pi}_K^0(\boldsymbol{\kappa} \boldsymbol{\Pi}_K^0(\nabla u_h)) \right) v \\
& + \sum_{K \in \Omega^h} \int_{\partial K} \left(\boldsymbol{\Pi}_K^0(\boldsymbol{\kappa} \boldsymbol{\Pi}_K^0(\nabla u_h)) \cdot \mathbf{n}_K \right) v. \tag{4.4}
\end{aligned}$$

The proof finishes by applying the boundary conditions (2.2a)-(2.2b) together with the discrete jump operator in (4.3)- (4.4), and subsequently substituting the result into (4.2). \square

In what follows, we will construct the reliability estimate for η .

Theorem 4.1. *If u and u_h solve the spectral problems (2.3) and (3.5), respectively, then the following result holds true*

$$|u - u_h|_{2,\Omega} \lesssim \eta + \frac{\lambda + \lambda_h}{2} |u - u_h|_{1,\Omega} + \|\boldsymbol{\kappa} \nabla u_h - \boldsymbol{\Pi}_K^0(\boldsymbol{\kappa} \nabla u_h)\|_{0,\Omega} + \|\nabla u_h - \boldsymbol{\Pi}_K^0(\nabla u_h)\|_{0,\Omega}.$$

Proof. Let us define $e := u - u_h \in V$ and $e_I \in V_h$. Then, for any $s \in \{2, 3\}$ and $t \in \{0, 1, \dots, s\}$, the following estimate holds

$$|e - e_I|_{t,\Omega} \lesssim h^{s-t} |e|_{s,\Omega}. \tag{4.5}$$

Testing the error equation in Lemma 4.1 by $v \equiv e - e_I \in V$ yields

$$\begin{aligned}
|e|_{2,\Omega}^2 & = a(e, e - e_I) + a(u, e_I) - a(u_h, e_I) + a^h(u_h, e_I) - a^h(u_h, e_I) \\
& = [\lambda b(u, e) - \lambda_h b(u_h, e)] + [\lambda_h \{b(u_h, e_I) - b^h(u_h, e_I)\}] + [a^h(u_h, e_I) - a(u_h, e_I)] \\
& + \sum_{K \in \Omega^h} a_K(\boldsymbol{\Pi}_K^{\nabla^2} u_h - u_h, e - e_I) \\
& + \lambda_h \sum_{K \in \Omega^h} \int_K (\boldsymbol{\kappa}(\nabla u_h - \boldsymbol{\Pi}_K^0(\nabla u_h))) \cdot \nabla(e - e_I) \\
& - \sum_{K \in \Omega^h} \int_K \lambda_h \operatorname{div} \left(\boldsymbol{\Pi}_K^0(\boldsymbol{\kappa} \boldsymbol{\Pi}_K^0(\nabla u_h)) \right) (e - e_I) \\
& - \sum_{f \in \mathcal{F}_\Omega^h} \int_f [(\nabla^2 \boldsymbol{\Pi}_K^{\nabla^2} u_h) \mathbf{n}_K^f] \cdot \nabla(e - e_I)
\end{aligned}$$

$$\begin{aligned}
& + \sum_{f \in \mathcal{F}_\Omega^h} \int_f [\lambda_h \mathbf{\Pi}_K^0(\boldsymbol{\kappa} \mathbf{\Pi}_K^0(\nabla u_h)) \cdot \mathbf{n}_K^f] (e - e_I) \\
& + \sum_{K \in \Omega^h} \int_K \lambda_h (\boldsymbol{\kappa} \mathbf{\Pi}_K^0(\nabla u_h) - \mathbf{\Pi}_K^0(\boldsymbol{\kappa} \mathbf{\Pi}_K^0(\nabla u_h))) \cdot \nabla(e - e_I) \\
& =: \sum_{j=1}^9 E_j,
\end{aligned} \tag{4.6}$$

where the error terms are defined by

$$\begin{aligned}
E_1 & := \lambda b(u, e) - \lambda_h b(u_h, e), \\
E_2 & := \lambda_h \{b(u_h, e_I) - b^h(u_h, e_I)\}, \\
E_3 & := a^h(u_h, e_I) - a(u_h, e_I), \\
E_4 & := \sum_{K \in \Omega^h} a_K(\mathbf{\Pi}_K^{\nabla^2} u_h - u_h, e - e_I), \\
E_5 & := \lambda_h \sum_{K \in \Omega^h} \int_K (\boldsymbol{\kappa}(\nabla u_h - \mathbf{\Pi}_K^0(\nabla u_h))) \cdot \nabla(e - e_I), \\
E_6 & := - \sum_{K \in \Omega^h} \int_K \lambda_h \operatorname{div}(\mathbf{\Pi}_K^0(\boldsymbol{\kappa} \mathbf{\Pi}_K^0(\nabla u_h))) (e - e_I), \\
E_7 & := - \sum_{f \in \mathcal{F}_\Omega^h} \int_f [(\nabla^2 \mathbf{\Pi}_K^{\nabla^2} u_h) \mathbf{n}_K^f] \cdot \nabla(e - e_I), \\
E_8 & := \sum_{f \in \mathcal{F}_\Omega^h} \int_f [\lambda_h \mathbf{\Pi}_K^0(\boldsymbol{\kappa} \mathbf{\Pi}_K^0(\nabla u_h)) \cdot \mathbf{n}_K^f] (e - e_I), \\
E_9 & := \sum_{K \in \Omega^h} \int_K \lambda_h (\boldsymbol{\kappa} \mathbf{\Pi}_K^0(\nabla u_h) - \mathbf{\Pi}_K^0(\boldsymbol{\kappa} \mathbf{\Pi}_K^0(\nabla u_h))) \cdot \nabla(e - e_I).
\end{aligned}$$

Notice that the terms E_3 , E_4 , and E_7 were estimated in [16, Theorem 14].

We now proceed to bound the remaining terms E_j , let $(\lambda, u) \neq (0, \mathbf{0})$ be an eigenpair of T , with a simple eigenvalue λ . For each mesh Ω^h , let (λ_h, u_h) be the corresponding discrete solution of the spectral problem, such that $|u_h|_{1, \Omega} = 1$ and satisfying

$$\lim_{h \rightarrow 0} |\lambda - \lambda_h| = 0 \quad \text{and} \quad \lim_{h \rightarrow 0} |u - u_h|_{2, \Omega} = 0.$$

Following the arguments presented in [16] and using the fact that $b(u, u) \lesssim 1$ in E_1 , we obtain

$$E_1 \lesssim \frac{\lambda + \lambda_h}{2} b(e, e) \lesssim \frac{\lambda + \lambda_h}{2} \|\mathbf{\Pi}_K^0 \nabla(u - u_h)\|_{0, \Omega}^2 \lesssim \frac{\lambda + \lambda_h}{2} |u - u_h|_{1, \Omega} |u - u_h|_{2, \Omega}. \tag{4.7}$$

Next, for the term E_2 , we apply the Lemma 3.2 to deduce

$$E_2 = \lambda_h \sum_{K \in \Omega^h} \int_K (\boldsymbol{\kappa} \nabla u_h - \mathbf{\Pi}_K^0(\boldsymbol{\kappa} \nabla u_h)) \cdot (\nabla e_I - \mathbf{\Pi}_K^0 \nabla e_I)$$

$$\begin{aligned}
&\lesssim \sum_{K \in \Omega^h} \|\kappa \nabla u_h - \mathbf{\Pi}_K^0(\kappa \nabla u_h)\|_{0,K} \|\nabla e_I - \mathbf{\Pi}_K^0 \nabla e_I\|_{0,K} \\
&\lesssim \|\kappa \nabla u_h - \mathbf{\Pi}_K^0(\kappa \nabla u_h)\|_{0,\Omega} |e - e_I|_{1,\Omega} \\
&\lesssim \|\kappa \nabla u_h - \mathbf{\Pi}_K^0(\kappa \nabla u_h)\|_{0,\Omega} |e - e_I|_{2,\Omega} \\
&\lesssim \|\kappa \nabla u_h - \mathbf{\Pi}_K^0(\kappa \nabla u_h)\|_{0,\Omega} |u - u_h|_{2,\Omega}.
\end{aligned} \tag{4.8}$$

In turn, for the terms E_5, E_6 y E_9 we apply the Cauchy-Schwarz inequality, estimate (4.5) and definitions (4.1a), (4.1b) and (4.1d) to obtain

$$\begin{aligned}
E_5 + E_6 + E_9 &\lesssim \sum_{K \in \Omega^h} \left\{ \|\nabla u_h - \mathbf{\Pi}_K^0(\nabla u_h)\|_{0,K} + h^2 \|\lambda_h \operatorname{div}(\mathbf{\Pi}_K^0(\kappa \mathbf{\Pi}_K^0(\nabla u_h)))\|_{0,K} \right. \\
&\quad \left. + h_K \|\lambda_h(\kappa \mathbf{\Pi}_K^0(\nabla u_h) - \mathbf{\Pi}_K^0(\kappa \mathbf{\Pi}_K^0(\nabla u_h)))\|_{0,K} \right\} |e|_{2,K} \\
&\lesssim \left\{ \|\nabla u_h - \mathbf{\Pi}_K^0(\nabla u_h)\|_{0,\Omega} + \Xi + \Lambda \right\} |u - u_h|_{2,\Omega}.
\end{aligned} \tag{4.9}$$

Lastly, for term E_8 we apply the standard trace inequality in the Sobolev space H^1 (see for instance [21]) and Cauchy-Schwarz inequality to obtain

$$E_8 \lesssim \mathcal{J} |u - u_h|_{2,\Omega}. \tag{4.10}$$

The result follows by inserting the estimates (4.7), (4.8), (4.9), (4.10), the inequalities [16, (39), (40) and (43)] into (4.6), and multiplying by $|u - u_h|_{2,\Omega}^{-1}$, i.e.,

$$|u - u_h|_{2,\Omega} \lesssim \eta + \frac{\lambda + \lambda_h}{2} |u - u_h|_{1,\Omega} + \|\kappa \nabla u_h - \mathbf{\Pi}_K^0(\kappa \nabla u_h)\|_{0,\Omega} + \|\nabla u_h - \mathbf{\Pi}_K^0(\nabla u_h)\|_{0,\Omega}.$$

□

Corollary 4.1. *If u and u_h solve the spectral problems (2.3) and (3.5), respectively. Then, the inequality holds*

$$|u - \mathbf{\Pi}_K^{\nabla^2} u_h|_{2,h} \lesssim \eta + \frac{\lambda + \lambda_h}{2} |u - u_h|_{1,\Omega} + \|\kappa \nabla u_h - \mathbf{\Pi}_K^0(\kappa \nabla u_h)\|_{0,\Omega} + \|\nabla u_h - \mathbf{\Pi}_K^0(\nabla u_h)\|_{0,\Omega}.$$

Proof. The proof follows by applying the triangle inequality, Theorem 4.1 and (4.1d). Indded,

$$\begin{aligned}
|u - \mathbf{\Pi}_K^{\nabla^2} u_h|_{2,h} &\leq |u - u_h|_{2,\Omega} + |u_h - \mathbf{\Pi}_K^{\nabla^2} u_h|_{2,h} \\
&\lesssim \eta + \frac{\lambda + \lambda_h}{2} |u - u_h|_{1,\Omega} + \|\kappa \nabla u_h - \mathbf{\Pi}_K^0(\kappa \nabla u_h)\|_{0,\Omega} \\
&\quad + \|\nabla u_h - \mathbf{\Pi}_K^0(\nabla u_h)\|_{0,\Omega} + \left\{ \sum_{K \in \Omega^h} S_K^2 \right\}^{1/2} \\
&\lesssim \eta + \frac{\lambda + \lambda_h}{2} |u - u_h|_{1,\Omega} + \|\kappa \nabla u_h - \mathbf{\Pi}_K^0(\kappa \nabla u_h)\|_{0,\Omega} + \|\nabla u_h - \mathbf{\Pi}_K^0(\nabla u_h)\|_{0,\Omega}.
\end{aligned}$$

□

Corollary 4.2. *If u and u_h solve the spectral problems (2.3) and (3.5), respectively. Then, the following estimate holds*

$$|\lambda - \lambda_h| \lesssim \left\{ \eta + \frac{\lambda + \lambda_h}{2} |u - u_h|_{1,\Omega} + \|\kappa \nabla u_h - \mathbf{\Pi}_K^0(\kappa \nabla u)\|_{0,\Omega} + \|\nabla u_h - \mathbf{\Pi}_K^0(\nabla u_h)\|_{0,\Omega} \right\}^2 \\ + \|\kappa \nabla u_h - \mathbf{\Pi}_K^0(\kappa \nabla u_h)\|_{0,\Omega} \|\nabla u_h - \mathbf{\Pi}_K^0(\nabla u_h)\|_{0,\Omega}.$$

Proof. The result follows by adding the term $|u - u_h|_{2,\Omega}^2 + \|\kappa \nabla u_h - \mathbf{\Pi}_K^0(\kappa \nabla u_h)\|_{0,\Omega} \|\nabla u_h - \mathbf{\Pi}_K^0(\nabla u_h)\|_{0,\Omega}$ to the square of the estimate in Corollary 4.1, and subsequently applying Theorem 3.1 together with Corollary 4.1. \square

Theorem 4.2. *If u and u_h solve the spectral problems (2.3) and (3.5), respectively, then there exists $h_0 > 0$ such that for all $h < h_0$ the following estimates hold true*

$$|u - u_h|_{2,\Omega} + |u - \mathbf{\Pi}_K^{\nabla^2} u_h|_{2,h} + \|\kappa \nabla u_h - \mathbf{\Pi}_K^0(\kappa \nabla u_h)\|_{0,\Omega} \|\nabla u_h - \mathbf{\Pi}_K^0(\nabla u_h)\|_{0,\Omega} \lesssim \eta, \quad (4.11)$$

$$|\lambda - \lambda_h| \lesssim \eta^2. \quad (4.12)$$

Proof. From Theorem 4.1, the definition of S_K (cf. (4.1d)) and Theorem 3.2 we have

$$|u - u_h|_{2,\Omega} + |u - \mathbf{\Pi}_K^{\nabla^2} u_h|_{2,h} + \|\kappa \nabla u_h - \mathbf{\Pi}_K^0(\kappa \nabla u_h)\|_{0,\Omega} \|\nabla u_h - \mathbf{\Pi}_K^0(\nabla u_h)\|_{0,\Omega} \\ \lesssim \eta + \frac{\lambda + \lambda_h}{2} |u - u_h|_{1,\Omega} + \|\kappa \nabla u_h - \mathbf{\Pi}_K^0(\kappa \nabla u)\|_{0,\Omega} + \|\nabla u_h - \mathbf{\Pi}_K^0(\nabla u_h)\|_{0,\Omega} \\ + \|\kappa \nabla u_h - \mathbf{\Pi}_K^0(\kappa \nabla u_h)\|_{0,\Omega} \|\nabla u_h - \mathbf{\Pi}_K^0(\nabla u_h)\|_{0,\Omega} \\ \lesssim \eta + \frac{\lambda + \lambda_h}{2} \left\{ |u - u_h|_{2,\Omega} + |u - \mathbf{\Pi}_K^{\nabla^2} u_h|_{2,h} \right\} + h^{1+s} \|\kappa \nabla u - \mathbf{\Pi}_K^0(\kappa \nabla u)\|_{0,\Omega} + |u - \mathcal{P}_h^\nabla u|_{1,\Omega} \\ + \|\kappa \nabla u_h - \mathbf{\Pi}_K^0(\kappa \nabla u)\|_{0,\Omega} + \|\nabla u_h - \mathbf{\Pi}_K^0(\nabla u_h)\|_{0,\Omega} \\ + \|\kappa \nabla u_h - \mathbf{\Pi}_K^0(\kappa \nabla u_h)\|_{0,\Omega} \|\nabla u_h - \mathbf{\Pi}_K^0(\nabla u_h)\|_{0,\Omega},$$

where, in the last line of the above inequality, we have proceeded as in [28, Theorem 4.4]. Thus, there exists $h_0 > 0$ such that for all $h < h_0$, the estimate (4.11) holds true.

Moreover, by applying Theorem 3.2, the estimate (4.11) and Corollary 4.2, there exists $h_0 > 0$ such that for all $0 < h < h_0$ the estimate (4.12) holds. \square

4.3. Efficiency

This subsection aims to prove the efficiency (lower bound for the error) of the global volume and jump estimators Ξ and \mathcal{J} up to the data oscillation Λ , the stabilisation estimator S and higher-order terms. We begin by recalling properties of element ψ_k and facet ψ_f bubble functions in the space $H_0^2(K)$ (see [34, Section 3.7] for construction details in two-dimensions and [16, Remark 6] for a discussion regarding the three-dimensional case).

$$\|q_K\|_{0,K}^2 \lesssim \int_K \psi_K q_K^2, \quad \forall q_K \in \mathbb{P}_2(K), \quad (4.13a)$$

$$\|\psi_K q_K\|_{0,K} \lesssim \|q_K\|_{0,K}, \quad \forall q_K \in \mathbb{P}_2(K), \quad (4.13b)$$

$$h_f^{-1} \|q_f\|_{0,f}^2 \lesssim \int_f q_f \mathbf{n}_K^f \cdot \nabla(\psi_f q_f), \quad \forall q_f \in \mathbb{P}_0(f), \quad (4.13c)$$

$$\|\mathbf{n}_K^f \cdot \nabla(\psi_f q_f)\|_{0,f} \lesssim h_f^{-1} \|q_f\|_{0,f}, \quad \forall q_f \in \mathbb{P}_0(f), \quad (4.13d)$$

$$\sum_{K=K^+,K^-} h_f^{-2} \|\psi_f q_f\|_{0,K} \lesssim \sum_{K=K^+,K^-} |\psi_f q_f|_{2,K}, \quad \forall q_f \in \mathbb{P}_0(f), \quad (4.13e)$$

$$\sum_{K=K^+,K^-} |\psi_f q_f|_{2,K} \lesssim \sum_{K=K^+,K^-} h_f^{-2} \|\psi_f q_f\|_{0,K}, \quad \forall q_f \in \mathbb{P}_0(f), \quad (4.13f)$$

$$\sum_{K=K^+,K^-} \|\psi_f q_f\|_{0,K} \lesssim h_f^{1/2} \|q_f\|_{0,f}, \quad \forall q_f \in \mathbb{P}_0(f). \quad (4.13g)$$

Moreover, the following local inverse estimates were established in [38]

$$|v|_{1,K} \lesssim h_K^{-1} |v|_{0,K} \quad \text{and} \quad |v|_{2,K} \lesssim h_K^{-2} |v|_{0,K}, \quad \forall v \in V_h^K. \quad (4.14)$$

The following result establishes an estimate for the volume estimator Ξ .

Lemma 4.2. *If u and u_h solve the spectral problems (2.3) and (3.5), respectively, then*

$$\Xi_K \lesssim |u - u_h|_{2,K} + S_K + h_K |\lambda u - \lambda_h u_h|_{1,K} + h_K \Lambda_K + h_K \|\nabla u_h - \mathbf{\Pi}_K^0(\nabla u_h)\|_{0,K}.$$

Proof. Let $K \in \Omega^h$. Consider ψ_K as the interior bubble function defined in K and $v_K := \psi_K \lambda_h \operatorname{div}(\mathbf{\Pi}_K^0(\boldsymbol{\kappa} \mathbf{\Pi}_K^0(\nabla u_h)))$. Since $v_K \in H_0^2(K)$, from now on we will denote its extension by v by zero in Ω . Thus, from the residual error equation in Lemma (4.1) we readily see that

$$\begin{aligned} \int_K \lambda_h \operatorname{div}(\mathbf{\Pi}_K^0(\boldsymbol{\kappa} \mathbf{\Pi}_K^0(\nabla u_h))) v &= \lambda b_K(u, v) - \lambda_h b_K(u_h, v) + a_K(\mathbf{\Pi}_K^{\nabla^2} u_h - u_h, v) - a_K(u - u_h, v) \\ &\quad + \lambda_h \int_K (\boldsymbol{\kappa}(\nabla u_h - \mathbf{\Pi}_K^0(\nabla u_h))) \cdot \nabla v \\ &\quad + \int_K \lambda_h (\boldsymbol{\kappa} \mathbf{\Pi}_K^0(\nabla u_h) - \mathbf{\Pi}_K^0(\boldsymbol{\kappa} \mathbf{\Pi}_K^0(\nabla u_h))) \cdot \nabla v \end{aligned}$$

Next, we apply (4.13a) in the previous identity to obtain

$$\begin{aligned} \|\lambda_h \operatorname{div}(\mathbf{\Pi}_K^0(\boldsymbol{\kappa} \mathbf{\Pi}_K^0(\nabla u_h)))\|_{0,K}^2 &\lesssim \int_K \psi_K [\lambda_h \operatorname{div}(\mathbf{\Pi}_K^0(\boldsymbol{\kappa} \mathbf{\Pi}_K^0(\nabla u_h)))]^2 \\ &= b(\lambda u - \lambda_h u_h, v) + a_K(\mathbf{\Pi}_K^{\nabla^2} u_h - u_h, v) - a(u - u_h, v) \\ &\quad + \lambda_h \int_K (\boldsymbol{\kappa}(\nabla u_h - \mathbf{\Pi}_K^0(\nabla u_h))) \cdot \nabla v \\ &\quad + \int_K \lambda_h (\boldsymbol{\kappa} \mathbf{\Pi}_K^0(\nabla u_h) - \mathbf{\Pi}_K^0(\boldsymbol{\kappa} \mathbf{\Pi}_K^0(\nabla u_h))) \cdot \nabla v \\ &\lesssim |\lambda u - \lambda_h u_h|_{1,K} |v|_{1,K} + |\mathbf{\Pi}_K^{\nabla^2} u_h - u_h|_{2,K} |v|_{2,K} \\ &\quad + |u - u_h|_{2,K} |v|_{2,K} + \|\nabla u_h - \mathbf{\Pi}_K^0(\nabla u_h)\|_{0,K} |v|_{1,K} \\ &\quad + \|\lambda_h (\boldsymbol{\kappa} \mathbf{\Pi}_K^0(\nabla u_h) - \mathbf{\Pi}_K^0(\boldsymbol{\kappa} \mathbf{\Pi}_K^0(\nabla u_h)))\|_{0,K} |v|_{1,K}. \quad (4.15) \end{aligned}$$

Since $v \in H_0^2(K)$, $0 \leq \psi_K \leq 1$ and $\lambda_h \operatorname{div}(\mathbf{\Pi}_K^0(\boldsymbol{\kappa} \mathbf{\Pi}_K^0(\nabla u_h))) \in \mathbb{P}_0(K) \in V_h$, the estimates (4.13b) and (4.14) lead to

$$|v|_{1,K} \lesssim h_K^{-1} \|\lambda_h \operatorname{div}(\mathbf{\Pi}_K^0(\boldsymbol{\kappa} \mathbf{\Pi}_K^0(\nabla u_h)))\|_{0,K}, \quad (4.16a)$$

$$|v|_{2,K} \lesssim h_K^{-2} \|\lambda_h \operatorname{div} (\mathbf{\Pi}_K^0(\boldsymbol{\kappa} \mathbf{\Pi}_K^0(\nabla u_h)))\|_{0,K}. \quad (4.16b)$$

Thus, by replacing the estimates (4.16a) and (4.16b) on the right-hand side of (4.15), and applying the definitions of Λ_K and S_K we have

$$\begin{aligned} \|\lambda_h \operatorname{div} (\mathbf{\Pi}_K^0(\boldsymbol{\kappa} \mathbf{\Pi}_K^0(\nabla u_h)))\|_{0,K} &\lesssim h_K^{-1} |\lambda u - \lambda_h u_h|_{1,K} + h_K^{-2} |\mathbf{\Pi}_K^{\nabla^2} u_h - u_h|_{2,K} \\ &\quad + h_K^{-2} |u - u_h|_{2,K} + h_K^{-1} \|\nabla u_h - \mathbf{\Pi}_K^0(\nabla u_h)\|_{0,K} \\ &\quad + h_K^{-1} \|\lambda_h (\boldsymbol{\kappa} \mathbf{\Pi}_K^0(\nabla u_h) - \mathbf{\Pi}_K^0(\boldsymbol{\kappa} \mathbf{\Pi}_K^0(\nabla u_h)))\|_{0,K} \\ &\lesssim h_K^{-1} |\lambda u - \lambda_h u_h|_{1,K} + h_K^{-2} S_K + h_K^{-1} \|\nabla u_h - \mathbf{\Pi}_K^0(\nabla u_h)\|_{0,K} \\ &\quad + h_K^{-2} |u - u_h|_{2,K} + h_K^{-1} \Lambda_K. \end{aligned}$$

Therefore, by using the definition of the local volume estimator Ξ_K and multiplying by h_K^2 in the above inequality, we obtain the result. \square

Now, the following result can be obtained following the arguments as those applied in [16, Lemma 19].

Lemma 4.3. *If u and u_h solve the spectral problems (2.3) and (3.5), respectively, then*

$$S_K \lesssim |u - u_h|_{2,K} + |u - \mathbf{\Pi}_K^{\nabla^2} u_h|_{2,K} + |u - u_h|_{1,K} + |u - \mathbf{\Pi}_K^{\nabla} u_h|_{1,K}.$$

The following result establishes an upper bound for the local jump estimator \mathcal{J}_f (cf. (4.1b)).

Lemma 4.4. *If u and u_h solve the spectral problems (2.3) and (3.5), respectively, then*

$$\begin{aligned} \mathcal{J}_f &\lesssim \sum_{K \in \Omega_f^h} \left\{ |u - u_h|_{2,K} + S_K + h_K |u - u_h|_{2,K} + (h_K + h_K^2) |\lambda u - \lambda_h u_h|_{1,K} \right. \\ &\quad \left. + (h_K + h_K^2) \|\nabla u_h - \mathbf{\Pi}_K^0(\nabla u_h)\|_{0,K} + h_K \Xi_K + (h_K + h_K^2) \Lambda_K + h_K S_K \right\} \\ &\quad + h_f^{5/2} \|[(\nabla^2 \mathbf{\Pi}_K^{\nabla^2} u_h) \mathbf{n}_K^f]\|_{0,f}. \end{aligned}$$

Proof. Given any facet $f \in \mathcal{F}^h$. Let us define ψ_l as the corresponding facet bubble function, and define the test functions $v_{1,f} := \psi_l [((\nabla^2 \mathbf{\Pi}_K^{\Delta} u_h) \mathbf{n}_K^l) \cdot \mathbf{n}_K^l]$, $v_{2,f} := \psi_l [\lambda_h \mathbf{\Pi}_K^0(\boldsymbol{\kappa} \mathbf{\Pi}_K^0(\nabla u_h)) \cdot \mathbf{n}_K^f] \in H_0^2(T^+ \cup T^-) \subset V$. Since $v_{i,f}$ ($i = 1, 2$) is a polynomial function, $v_{i,f}$ can be extended to $K^+ \cup K^-$, where $K^+, K^- \in \Omega_h$ have f as a common facet. Without losing generality, this extension is denoted by v_i .

First, note that the estimates (4.14) and (4.13g), together with ((M3)) lead to

$$|v_i|_{1,K} \lesssim h_f^{-1/2} \|q_i\|_{0,K}, \quad (4.17a)$$

$$|v_i|_{2,K} \lesssim h_f^{-3/2} \|q_i\|_{0,K}. \quad (4.17b)$$

where $i = 1, 2$, $q_1 = [((\nabla^2 \mathbf{\Pi}_K^{\Delta} u_h) \mathbf{n}_K^l) \cdot \mathbf{n}_K^l]$, and $q_2 = [\lambda_h \mathbf{\Pi}_K^0(\boldsymbol{\kappa} \mathbf{\Pi}_K^0(\nabla u_h)) \cdot \mathbf{n}_K^f]$.

Next, the identities in [16, (22)-(24)], together with Lemma 4.1 and (4.13c) imply that

$$h_f^{-1} \|[(\nabla^2 \mathbf{\Pi}_K^{\nabla^2} u_h) \mathbf{n}_K^f]\|_{0,f}^2 \lesssim \int_f [(\nabla^2 \mathbf{\Pi}_K^{\nabla^2} u_h) \mathbf{n}_K^f] \cdot \nabla v_1$$

$$\begin{aligned}
&= \sum_{K \in \Omega_f^h} \left\{ a_K(u_h - u, v_1) + \lambda b_K(u, v_1) - \lambda_h b_K(u_h, v_1) \right. \\
&\quad + a_K(\Pi_K^{\nabla^2} u_h - u_h, v_1) \\
&\quad + \lambda_h \int_K (\boldsymbol{\kappa}(\nabla u_h - \Pi_K^0(\nabla u_h))) \cdot \nabla v_1 \\
&\quad - \int_K \lambda_h \operatorname{div}(\Pi_K^0(\boldsymbol{\kappa} \Pi_K^0(\nabla u_h))) v_1 \\
&\quad \left. + \int_K \lambda_h (\boldsymbol{\kappa} \Pi_K^0(\nabla u_h) - \Pi_K^0(\boldsymbol{\kappa} \Pi_K^0(\nabla u_h))) \cdot \nabla v_1 \right\} \\
&\quad + \int_f \llbracket \lambda_h \Pi_K^0(\boldsymbol{\kappa} \Pi_K^0(\nabla u_h)) \cdot \mathbf{n}_K^f \rrbracket v_1 \\
&\lesssim \sum_{K \in \Omega_f^h} \left\{ |u - u_h|_{2,K} |v_1|_{2,K} + |\lambda u - \lambda_h u_h|_{1,K} |v_1|_{1,K} \right. \\
&\quad + |u_h - \Pi_K^{\nabla^2} u_h|_{2,K} |v_1|_{2,K} + \|\nabla u_h - \Pi_K^0(\nabla u_h)\|_{0,K} |v_1|_{1,K} \\
&\quad + \|\lambda_h \operatorname{div}(\Pi_K^0(\boldsymbol{\kappa} \Pi_K^0(\nabla u_h)))\|_{0,K} \|v_1\|_{0,K} \\
&\quad + \|\lambda_h (\boldsymbol{\kappa} \Pi_K^0(\nabla u_h) - \Pi_K^0(\boldsymbol{\kappa} \Pi_K^0(\nabla u_h)))\|_{0,K} |v_1|_{1,K} \left. \right\} \\
&\quad + \|\llbracket \lambda_h \Pi_K^0(\boldsymbol{\kappa} \Pi_K^0(\nabla u_h)) \cdot \mathbf{n}_K^f \rrbracket\|_{0,f} \|v_1\|_{0,f}.
\end{aligned}$$

Inserting (4.17a) and (4.17a) in the previous inequality and multiplying by $h^{3/2}$, lead to

$$\begin{aligned}
h_f^{1/2} \|\llbracket (\nabla^2 \Pi_K^{\nabla^2} u_h) \mathbf{n}_K^f \rrbracket\|_{0,f} &\lesssim \sum_{K \in \Omega_f^h} \left\{ |u - u_h|_{2,K} + h_f |\lambda u - \lambda_h u_h|_{1,K} \right. \\
&\quad \left. + h_f \|\nabla u_h - \Pi_K^0(\nabla u_h)\|_{0,K} + \Xi_K + h_f \Lambda_K + S_K \right\} \\
&\quad + h_f^{3/2} \|\llbracket \lambda_h \Pi_K^0(\boldsymbol{\kappa} \Pi_K^0(\nabla u_h)) \cdot \mathbf{n}_K^f \rrbracket\|_{0,f}. \tag{4.18}
\end{aligned}$$

Similarly, we use Lemma 4.1 and (4.13c) to arrive at

$$\begin{aligned}
h_f^{-1} \|\llbracket \lambda_h \Pi_K^0(\boldsymbol{\kappa} \Pi_K^0(\nabla u_h)) \cdot \mathbf{n}_K^f \rrbracket\|_{0,f}^2 &\lesssim \int_f \llbracket \lambda_h \Pi_K^0(\boldsymbol{\kappa} \Pi_K^0(\nabla u_h)) \cdot \mathbf{n}_K^f \rrbracket v_2 \\
&= \sum_{K \in \Omega_f^h} \left\{ a_K(u_h - u, v_2) + \lambda b_K(u, v_2) - \lambda_h b_K(u_h, v_2) \right. \\
&\quad + a_K(\Pi_K^{\nabla^2} u_h - u_h, v_2) \\
&\quad + \lambda_h \int_K (\boldsymbol{\kappa}(\nabla u_h - \Pi_K^0(\nabla u_h))) \cdot \nabla v_2 \\
&\quad \left. - \int_K \lambda_h \operatorname{div}(\Pi_K^0(\boldsymbol{\kappa} \Pi_K^0(\nabla u_h))) v_2 \right\}
\end{aligned}$$

$$\begin{aligned}
& + \int_K \lambda_h (\boldsymbol{\kappa} \boldsymbol{\Pi}_K^0(\nabla u_h) - \boldsymbol{\Pi}_K^0(\boldsymbol{\kappa} \boldsymbol{\Pi}_K^0(\nabla u_h))) \cdot \nabla v_2 \Big\} \\
& + \int_f \llbracket (\nabla^2 \boldsymbol{\Pi}_K^{\nabla^2} u_h) \mathbf{n}_K^f \rrbracket \cdot \nabla v_2 \\
\lesssim & \sum_{K \in \Omega_f^h} \left\{ |u - u_h|_{2,K} |v_2|_{2,K} + |\lambda u - \lambda_h u_h|_{1,K} |v_2|_{1,K} \right. \\
& + |u_h - \boldsymbol{\Pi}_K^{\nabla^2} u_h|_{2,K} |v_2|_{2,K} + \|\nabla u_h - \boldsymbol{\Pi}_K^0(\nabla u_h)\|_{0,K} |v_2|_{1,K} \\
& + \|\lambda_h \operatorname{div}(\boldsymbol{\Pi}_K^0(\boldsymbol{\kappa} \boldsymbol{\Pi}_K^0(\nabla u_h)))\|_{0,K} \|v_2\|_{0,K} \\
& + \|\lambda_h (\boldsymbol{\kappa} \boldsymbol{\Pi}_K^0(\nabla u_h) - \boldsymbol{\Pi}_K^0(\boldsymbol{\kappa} \boldsymbol{\Pi}_K^0(\nabla u_h)))\|_{0,K} \|v\|_{1,K} \\
& \left. + \|\llbracket \lambda_h \boldsymbol{\Pi}_K^0(\boldsymbol{\kappa} \boldsymbol{\Pi}_K^0(\nabla u_h)) \cdot \mathbf{n}_K^f \rrbracket\|_{0,f} \|v_2\|_{0,f} \right\}.
\end{aligned}$$

Thus,

$$\begin{aligned}
h_f^{3/2} \|\llbracket \lambda_h \boldsymbol{\Pi}_K^0(\boldsymbol{\kappa} \boldsymbol{\Pi}_K^0(\nabla u_h)) \cdot \mathbf{n}_K^f \rrbracket\|_{0,f} & \lesssim \sum_{K \in \Omega_f^h} \left\{ h_f |u - u_h|_{2,K} + h_f^2 |\lambda u - \lambda_h u_h|_{1,K} \right. \\
& \left. + h_f^2 \|\nabla u_h - \boldsymbol{\Pi}_K^0(\nabla u_h)\|_{0,K} + h_f \Xi_K + h_f^2 \Lambda_K + h_f S_K \right\} \\
& + h_f^{5/2} \|\llbracket (\nabla^2 \boldsymbol{\Pi}_K^{\nabla^2} u_h) \mathbf{n}_K^f \rrbracket\|_{0,f}. \tag{4.19}
\end{aligned}$$

The result follows from the addition of (4.18) and (4.19), together with Lemma 4.2 and the inequality $h_f \leq h_K$. \square

Finally, we introduce the efficiency result of the global volume and jump estimators (up to data oscillation, stabilisation, and higher-order terms) as a direct consequence of Lemmas 4.2-4.4 and summation for all $K \in \Omega^h$.

Theorem 4.3. *If u and u_h solve the spectral problems (2.3) and (3.5), respectively. Then,*

$$\Xi + \mathcal{J} \lesssim |u - u_h|_{2,\Omega} + S + \text{HOTs},$$

where the higher-order terms are given by

$$\begin{aligned}
\text{HOTs} & := (h + h^2) |\lambda u - \lambda_h u_h|_{1,\Omega} + (h + h^2) \|\nabla u_h - \boldsymbol{\Pi}_K^0(\nabla u_h)\|_{0,\Omega} + h \Xi + (h + h^2) \Lambda + h S \\
& + \sum_{f \in \mathcal{F}_\Omega^h} h_f^{5/2} \|\llbracket (\nabla^2 \boldsymbol{\Pi}_K^{\nabla^2} u_h) \mathbf{n}_K^f \rrbracket\|_{0,f}.
\end{aligned}$$

5. Numerical results

This section presents several numerical experiments showing the performance of the estimator introduced in Section 4. We test the behaviour of the estimator under uniform and adaptive refinement for a variety of polytopal meshes. Finally, we study the applicability of the adaptive routine with an application-oriented problem.

The method is implemented in the library `vem++` formally introduced in [15] and the generalised eigenvalue problem arising from such discretisations is solved inside `vem++` with the library `SLEPC` (cf. [23]). We follow the standard strategy

SOLVE → ESTIMATE → MARK → REFINE.

We adopt two alternatives for the REFINE stage: the two dimensional adaptive refinement uses the Matlab-based method from [37], connecting each edge mid-point to the polygon barycenter. On the other hand, the three dimensional routine employs the library `p4est` [9] through the `GridapP4est` module of the Julia package `Gridap` [4]. While restricted to cubical meshes, `p4est` supports the generation of hanging nodes, which are naturally handled by the VEM. It is worth noting that the refinement strategy does not rely on the specific features of `vem++`. As a consequence, the proposed implementation can be applied to more general (possibly non-convex) polytopal meshes, provided that a suitable refinement routine is chosen. In addition, we employ a Dörfler/Bulk marking strategy as follows: mark the subset of mesh elements $\Omega_*^h \subseteq \Omega^h$ with the largest estimated errors such that for $\delta_* = \frac{1}{2} \in [0, 1]$, we have

$$\delta_* \sum_{K \in \Omega^h} \eta_K^2 \leq \sum_{K \in \Omega_*^h} \eta_K^2.$$

The experimental order of convergence $r_{j+1}(\ast)$ against the total number of degrees of freedom #DoFs and the effectivity index eff are computed as follows

$$r(\ast)_{j+1} = -d \frac{\log\left(\frac{\ast_{j+1}}{\ast_j}\right)}{\log\left(\frac{\#\text{DoFs}_{j+1}}{\#\text{DoFs}_j}\right)}, \quad \text{eff}_j = \frac{(\eta_i^2)_j}{(e_{i,h})_j},$$

where η_i and $e_{i,h} = |\lambda_{i,h} - \lambda_i|$ are the error and global total error estimator associated to the i -th eigenvalue (same notation holds for all the contributing terms of the error estimator cf. (4.1)). It is worth noting that the convergence rate holds for the errors and for the global error estimator, together with each of its constituent terms. Finally, we remark that the stabilisation operator can be modified by introduce a coefficient α as follows:

$$\alpha S_K^{\nabla^2}(u_h - \Pi_K^{\nabla^2} u_h, u_h - \Pi_K^{\nabla^2} u_h).$$

The influence of the parameters α on the accuracy of the scheme was previously addressed in [30] through a sensitivity analysis (see also [16]). In particular, we select the DOFI-DOFI type of stabilisation as in [29] and $\alpha = 1$ for both 2D and 3D case.

5.1. Example 1. The estimator under uniform refinement

This test solves the buckling eigenvalue problem (2.1) with the plane stress tensor taken as the identity ($\kappa = \mathbb{I}_{d \times d}$), focusing on the first eigenvalue λ_1 in both two and three dimension. We consider the unit square $\Omega = (0, 1)^2$ under a variety of discretisations (see Figure 1(a)-1(c)) with boundary **CP** boundary conditions (cf. (2.2b)) and the unit cube $\Omega = (0, 1)^3$ with the discretisation shown in Figure 1(d) and **SSP** conditions as in (2.2a), the stabilisation parameter is set to unity value.

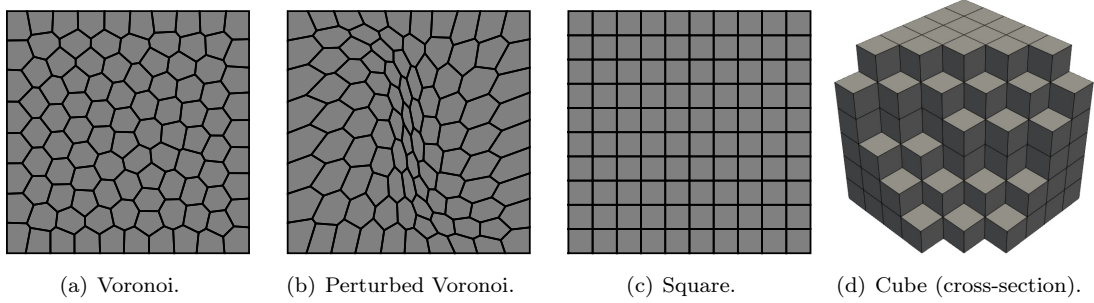


Figure 1: Example 1. Polytopal discretisations used for the uniform refinement test.

It is well known that the lowest buckling coefficient of the proposed 2D problem is given by $\lambda_1 \approx 5.3037$ (see e.g. [27]) with $L = 1$ and $D = \pi^2$. Whereas, the associated lowest eigenvalue for the 3D has an exact value of $\lambda_1 = 3\pi^2$ for $L, D = 1$ (cf. [17]). Note that, the convexity of the considered domains ensures the smoothness of the associated eigenfunction u_1 . Therefore, the optimal convergence rate is recovered for the error $e_{1,h}$, and the global error estimator η (see Table 1-2). Moreover, for any $K \in \Omega^h$ and constant κ , the local data oscillation Λ_K (cf. (4.1c)) is exactly zero since $\kappa \nabla \Pi_K^\nabla u_h = \Pi_K^\nabla(\kappa \nabla \Pi_K^\nabla u_h)$, confirmed experimentally in both 2D and 3D cases.

The convergence history of the eigenvalue error $e_{1,h}$ together with the global error estimator η under (two-dimensional) uniform refinement is reported in Table 1. Whereas, the three dimensional behaviour (associated with the eigenvalue error $e_{1,h}$) is summarised in Table 2, for this particular case, the dominant terms of the estimator (\mathcal{J} and \mathcal{S}) decay slower than Ξ , indicating optimal performance of the estimator once the mesh is sufficiently fine (results for very fine meshes are omitted due to the high computational cost). The reliability of the estimator is confirmed (see Theorem 4.2) and the expected convergence rate of $O(h^2)$ is achieved (cf. Theorem 3.1) for both experiments. Finally, the effectivity index eff remains bounded for each test case as predicted by Theorem 4.3.

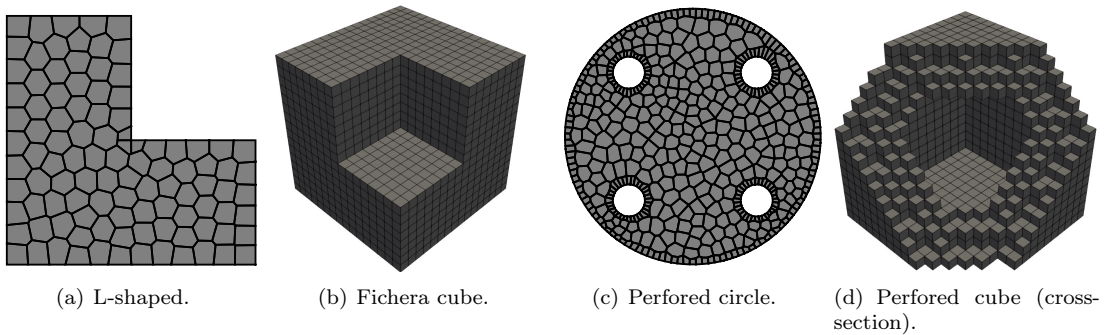


Figure 2: Example 2. Polytopal discretisations used for the adaptive refinement test.

Ω^h	#DoFs	$e_{1,h}$	$r(e_{1,h})$	η^2	$r(\eta^2)$	Ξ^2	$r(\Xi^2)$	\mathcal{J}^2	$r(\mathcal{J}^2)$	S^2	$r(S^2)$	Λ^2	$r(\Lambda^2)$	eff
Voronoi	606	3.11e-01	*	9.22e+00	*	7.28e-01	*	4.80e+00	*	3.69e+00	*	8.38e-33	*	2.97e+01
	2406	1.23e-01	1.34e+00	2.61e+00	1.83e+00	5.28e-02	3.81e+00	1.22e+00	1.99e+00	1.34e+00	1.47e+00	2.04e-33	*	2.12e+01
	5406	6.62e-02	1.53e+00	1.30e+00	1.72e+00	1.04e-02	4.02e+00	6.02e-01	1.75e+00	6.91e-01	1.63e+00	9.02e-34	*	1.97e+01
	9597	3.94e-02	1.81e+00	7.59e-01	1.88e+00	3.31e-03	3.98e+00	3.49e-01	1.90e+00	4.06e-01	1.85e+00	5.10e-34	*	1.92e+01
	14997	2.33e-02	2.37e+00	4.66e-01	2.19e+00	1.44e-03	3.74e+00	2.21e-01	2.05e+00	2.44e-01	2.29e+00	3.22e-34	*	2.00e+01
	21594	1.63e-02	1.95e+00	3.21e-01	2.05e+00	6.80e-04	4.10e+00	1.54e-01	1.98e+00	1.66e-01	2.10e+00	2.16e-34	*	1.97e+01
	29394	1.37e-02	1.11e+00	2.52e-01	1.58e+00	3.70e-04	3.95e+00	1.16e-01	1.84e+00	1.35e-01	1.33e+00	1.68e-34	*	1.83e+01
	38364	1.12e-02	1.52e+00	1.95e-01	1.90e+00	2.21e-04	3.85e+00	8.80e-02	2.06e+00	1.07e-01	1.77e+00	1.26e-34	*	1.74e+01
	48579	9.21e-03	1.66e+00	1.56e-01	1.89e+00	1.28e-04	4.63e+00	6.93e-02	2.03e+00	8.68e-02	1.77e+00	9.69e-35	*	1.70e+01
	59976	7.40e-03	2.08e+00	1.25e-01	2.09e+00	8.75e-05	3.63e+00	5.71e-02	1.85e+00	6.82e-02	2.29e+00	8.21e-35	*	1.69e+01
Avg.	*	*	1.71e+00	*	1.90e+00	*	3.97e+00	*	1.94e+00	*	1.83e+00	*	*	1.99e+01
Perturbed Voronoi	606	1.63e+00	*	1.37e+01	*	6.97e-01	*	3.08e+00	*	9.88e+00	*	7.98e-33	*	8.39e+00
	2406	6.66e-01	1.30e+00	6.48e+00	1.08e+00	1.77e-01	1.99e+00	1.11e+00	1.48e+00	5.19e+00	9.34e-01	2.63e-33	*	9.72e+00
	5406	3.29e-01	1.74e+00	3.40e+00	1.59e+00	4.02e-02	3.66e+00	5.62e-01	1.69e+00	2.80e+00	1.53e+00	1.29e-33	*	1.03e+01
	9597	2.04e-01	1.68e+00	2.15e+00	1.59e+00	1.59e-02	3.23e+00	3.50e-01	1.65e+00	1.79e+00	1.56e+00	6.88e-34	*	1.06e+01
	14997	1.30e-01	2.03e+00	1.39e+00	1.96e+00	6.28e-03	4.16e+00	2.27e-01	1.94e+00	1.16e+00	1.94e+00	4.78e-34	*	1.07e+01
	21594	9.27e-02	1.84e+00	1.00e+00	1.81e+00	3.38e-03	3.40e+00	1.66e-01	1.73e+00	8.31e-01	1.82e+00	3.31e-34	*	1.08e+01
	29394	7.08e-02	1.75e+00	7.62e-01	1.76e+00	1.84e-03	3.96e+00	1.22e-01	1.99e+00	6.38e-01	1.71e+00	2.41e-34	*	1.08e+01
	38364	5.51e-02	1.89e+00	5.89e-01	1.93e+00	1.19e-03	3.28e+00	9.47e-02	1.90e+00	4.93e-01	1.94e+00	1.93e-34	*	1.07e+01
	48579	4.38e-02	1.94e+00	4.69e-01	1.93e+00	6.62e-04	4.94e+00	7.51e-02	1.96e+00	3.93e-01	1.92e+00	1.45e-34	*	1.07e+01
	59976	3.64e-02	1.75e+00	3.89e-01	1.76e+00	4.37e-04	3.94e+00	6.27e-02	1.71e+00	3.26e-01	1.77e+00	1.22e-34	*	1.07e+01
Avg.	*	*	1.77e+00	*	1.71e+00	*	3.62e+00	*	1.78e+00	*	1.68e+00	*	*	1.03e+01
Square	363	4.56e-01	*	1.45e+01	*	1.54e+00	*	8.90e+00	*	4.04e+00	*	3.76e-33	*	3.17e+01
	1323	1.34e-01	1.90e+00	3.92e+00	2.02e+00	1.31e-01	3.82e+00	2.54e+00	1.94e+00	1.25e+00	1.81e+00	1.34e-33	*	2.93e+01
	2883	6.15e-02	2.00e+00	1.78e+00	2.03e+00	2.76e-02	4.00e+00	1.17e+00	2.00e+00	5.82e-01	1.96e+00	6.65e-34	*	2.89e+01
	5043	3.50e-02	2.01e+00	1.01e+00	2.03e+00	8.93e-03	4.03e+00	6.65e-01	2.01e+00	3.33e-01	2.00e+00	2.89e-34	*	2.87e+01
	7803	2.26e-02	2.01e+00	6.47e-01	2.03e+00	3.70e-03	4.04e+00	4.28e-01	2.01e+00	2.15e-01	2.01e+00	2.35e-34	*	2.87e+01
	11163	1.57e-02	2.01e+00	4.50e-01	2.02e+00	1.79e-03	4.04e+00	2.99e-01	2.01e+00	1.50e-01	2.01e+00	1.55e-34	*	2.86e+01
	15123	1.16e-02	2.01e+00	3.31e-01	2.02e+00	9.71e-04	4.04e+00	2.20e-01	2.01e+00	1.10e-01	2.01e+00	1.04e-34	*	2.85e+01
	19683	8.92e-03	2.00e+00	2.54e-01	2.02e+00	5.71e-04	4.04e+00	1.69e-01	2.01e+00	8.46e-02	2.01e+00	7.36e-35	*	2.85e+01
	24843	7.07e-03	2.00e+00	2.01e-01	2.02e+00	3.57e-04	4.03e+00	1.34e-01	2.01e+00	6.70e-02	2.01e+00	6.64e-35	*	2.84e+01
	30603	5.74e-03	1.99e+00	1.63e-01	2.02e+00	2.34e-04	4.03e+00	1.08e-01	2.01e+00	5.43e-02	2.01e+00	6.04e-35	*	2.84e+01
Avg.	*	*	1.99e+00	*	2.02e+00	*	4.01e+00	*	2.00e+00	*	1.98e+00	*	*	2.90e+01

Table 1: Example 1. Convergence history for a variety of 2D meshes of the eigenvalue error $e_{1,h} = |\lambda_{1,h} - \lambda_1|$, and the global error estimator η^2 together with the volume residual, jump residual, stabilisation and data oscillation terms Ξ^2 , \mathcal{J}^2 , S^2 , and Λ^2 . The effectivity index eff of the estimator is also shown in the last column.

Ω^h	#DoFs	$e_{1,h}$	$r(e_{1,h})$	η^2	$r(\eta^2)$	Ξ^2	$r(\Xi^2)$	\mathcal{J}^2	$r(\mathcal{J}^2)$	S^2	$r(S^2)$	Λ^2	$r(\Lambda^2)$	eff
Cube	1372	3.82e+00	*	8.29e+01	*	7.41e+01	*	6.74e+00	*	2.03e+00	*	6.76e-31	*	2.17e+01
	5324	1.92e+00	1.53e+00	1.79e+01	3.39e+00	1.49e+01	3.55e+00	1.79e+00	2.94e+00	1.21e+00	1.14e+00	1.97e-31	*	9.33e+00
	13500	1.06e+00	1.90e+00	6.32e+00	3.36e+00	4.76e+00	3.68e+00	8.27e-01	2.48e+00	7.33e-01	1.62e+00	1.59e-31	*	5.93e+00
	27436	6.70e-01	1.96e+00	2.87e+00	3.34e+00	1.91e+00	3.86e+00	4.78e-01	2.32e+00	4.79e-01	1.80e+00	9.04e-32	*	4.28e+00
	48668	4.58e-01	1.99e+00	1.54e+00	3.24e+00	8.99e-01	3.95e+00	3.11e-01	2.24e+00	3.34e-01	1.88e+00	6.30e-32	*	3.38e+00
	78732	3.32e-01	2.01e+00	9.38e-01	3.11e+00	4.74e-01	3.99e+00	2.19e-01	2.19e+00	2.45e-01	1.93e+00	4.87e-32	*	2.83e+00
	119164	2.51e-01	2.02e+00	6.22e-01	2.98e+00	2.73e-01	4.01e+00	1.63e-01	2.16e+00	1.87e-01	1.96e+00	2.56e-32	*	2.48e+00
	171500	1.96e-01	2.02e+00	4.40e-01	2.86e+00	1.67e-01	4.02e+00	1.26e-01	2.13e+00	1.47e-01	1.98e+00	2.46e-32	*	2.24e+00
	Avg.	*	*	1.92e+00	*	3.18e+00	*	3.87e+00	*	2.35e+00	*	1.76e+00	*	*

Table 2: Example 1. Convergence history for the 3D cube mesh of the eigenvalue error $e_{1,h} = |\lambda_{1,h} - \lambda_1|$, and the global error estimator η^2 together with the volume residual, jump residual, stabilisation and data oscillation terms Ξ^2 , \mathcal{J}^2 , S^2 , and Λ^2 . The effectivity index eff of the estimator is also shown in the last column.

5.2. *Example 2. The estimator under adaptive refinement*

In this experiment we consider (2.1) loaded in the x -direction by a linearly distributed in-plane traction, i.e. the plane stress tensor function is given by

$$\boldsymbol{\kappa}_{2D} = \begin{pmatrix} 1 - \kappa_0 y & 0 \\ 0 & 0 \end{pmatrix} \quad \text{and} \quad \boldsymbol{\kappa}_{3D} = \begin{pmatrix} 1 - \kappa_0 y & 0 & 0 \\ 0 & 0 & 0 \\ 0 & 0 & 0 \end{pmatrix}, \quad \text{with} \quad \kappa_0 \in \left\{ 0, \frac{2}{3}, 1, \frac{4}{3} \right\}.$$

We begin by examining the classical L-shaped and Fichera cube domains (shown in Figs 2(a)-2(b)), given by $\Omega = (0, 1)^2 \setminus (1/2, 1)^2$ and $\Omega = (0, 1)^3 \setminus (1/2, 1)^3$. For this test, **CP** boundary conditions are imposed and the parameter κ_0 is set to 0 for the two-dimensional and 2/3 for the three-dimensional case. Exact eigenvalues for the L-shaped domain in the isotropic case $\boldsymbol{\kappa} = \mathbb{I}_{d \times d}$ are available in the literature [28].

The second part of this test considers perforated domains. The two-dimensional domain consist on a circle centred in $(1/2, 1/2)$ with radius $1/2$, the perforations are given by four circles with radius $1/16$ centred at $(1/4, 1/4)$, $(1/4, 3/4)$, $(3/4, 1/4)$, and $(3/4, 3/4)$ (see Fig 2(c)). Whereas, the three-dimensional domain is given by $(0, 1)^3 \setminus (1/4, 3/4)^3$, a unit cube domain perforated with an inner cube (cf. Fig 2(d)). In this test, we impose **SSP** conditions on the outer boundary and is set free in the perforations, the respective values for κ_0 are set to 1 and $4/3$. The first eigenvalue for a similar perforated circle domain (i.e. the perforations are located in different positions) in the isotropic case $\boldsymbol{\kappa} = \mathbb{I}_{d \times d}$ and **CP**-free boundary conditions is available in [1].

Note that the non-convexity of the domains proposed, together with the presence of perforations, naturally calls for adaptive refinement routines. These geometric features generate singularities at re-entrant corners and around internal boundaries, and adaptive refinement provides an efficient way to recover optimal accuracy while avoiding unnecessary global mesh refinement. We recall that to the best of the authors' knowledge, no exact eigenvalues have been reported for the configurations proposed in this numerical example, which here are compute with the values $D, L = 1$.

Table 3 summarise the convergence history of the global error estimator η_i ($i = 1, 2, 3$) under adaptive refinement. We recover the convergence rate predicted by Theorem 3.1 for all the tested values of κ_0 and meshes shown in Fig 2. Moreover, the eigenvalues $\lambda_{i,h}$ obtained by our scheme are displayed in Table 3 for each refinement step and the snapshot of the associated eigenfunctions for each test case are shown in Figs 3,4,5, and 6, respectively.

On the other hand, we observe that the marking procedure is inherently tied to the eigenvalue we are interested in. For example, in the perforated cube section of Table 3, the third eigenvalue computed by the scheme in the last refinement step has a value of 164.6964, which is larger than the first eigenvalue 70.17242. These values appear directly in the global volume estimator Ξ and the global jump estimator \mathcal{J} . Then, when targeting the third eigenvalue, fewer elements need to be included in \mathcal{T}_*^h in order to meet the criterion required by the Dⁿorfler/Bulk marking strategy. This explains why four refinement steps for the first eigenvalue produce 150 684 total DoFs, whereas five refinement steps for the third eigenvalue yield only 134 967 total DoFs.

5.3. *Example 3. Buckling behaviour of turbine blades and the influence of internal air-cooling passages*

While Section 5.2 investigated perforated domains purely from a numerical analysis standpoint (cf. Figs 2(c), 2(d)), this example illustrates their relevance in a engineering-type application.

κ_0	Ω^h	#DoFs	$\lambda_{1,h}$	η_1^2	$r(\eta_1^2)$	#DoFs	$\lambda_{2,h}$	η_2^2	$r(\eta_2^2)$	#DoFs	$\lambda_{3,h}$	η_3^2	$r(\eta_3^2)$	
0	L-shaped	21618	171.59229	7.64e+00	*	21618	257.95567	1.82e+01	*	21618	284.78435	1.69e+01	*	
		28032	174.17526	4.65e+00	3.82e+00	28896	264.14787	1.16e+01	3.11e+00	33693	290.21865	1.03e+01	2.25e+00	
		38547	175.50164	2.68e+00	3.46e+00	40839	267.53076	6.89e+00	3.01e+00	47931	292.98084	5.95e+00	3.09e+00	
		54630	176.26211	1.51e+00	3.30e+00	56997	269.49691	4.02e+00	3.24e+00	71622	294.89883	3.30e+00	2.94e+00	
		88581	176.91846	8.45e-01	2.40e+00	93060	270.94045	2.22e+00	2.43e+00	124317	296.28080	1.69e+00	2.41e+00	
		137970	177.34288	4.70e-01	2.64e+00	146022	271.77504	1.23e+00	2.62e+00	191100	296.93796	9.46e-01	2.71e+00	
		219516	177.51347	2.82e-01	2.20e+00	219957	272.20495	7.29e-01	2.54e+00	296409	297.25558	5.86e-01	2.18e+00	
		366699	177.67225	1.73e-01	1.90e+00	364734	272.55606	4.55e-01	1.87e+00	514893	297.61744	3.57e-01	1.79e+00	
		Avg.	*	*	*	2.70e+00	*	*	*	2.69e+00	*	*	*	2.48e+00
		3/2	Fichera cube	17604	87.64595	4.07e+01	*	17604	124.34059	1.34e+02	*	17604	151.83164	1.81e+02
31940	93.63479			2.97e+01	1.58e+00	32252	145.80585	1.10e+02	1.00e+00	38840	160.73295	1.39e+02	1.01e+00	
55084	97.62630			1.96e+01	2.30e+00	59324	154.18331	6.93e+01	2.25e+00	54120	173.03266	8.01e+01	4.96e+00	
111972	100.76571			1.32e+01	1.67e+00	99188	163.33531	4.85e+01	2.09e+00	83320	182.78053	5.96e+01	2.06e+00	
245936	103.50021			9.08e+00	1.42e+00	220916	171.40649	2.98e+01	1.82e+00	163480	192.79947	4.16e+01	1.59e+00	
Avg.	*			*	*	1.74e+00	*	*	*	1.79e+00	*	*	*	2.41e+00
1	Perforated circle	3147	100.38706	2.79e-01	*	3147	119.70873	3.63e-01	*	3147	177.87490	5.59e-01	*	
		4077	108.57435	1.89e-01	3.00e+00	3945	132.72194	2.41e-01	3.61e+00	3777	203.42516	4.03e-01	3.58e+00	
		5547	117.77372	1.21e-01	2.89e+00	5715	146.84074	1.59e-01	2.27e+00	4800	229.51096	2.71e-01	3.33e+00	
		8484	122.67488	7.70e-02	2.13e+00	9225	155.03149	1.00e-01	1.92e+00	7296	252.59657	2.19e-01	1.02e+00	
		13881	125.24802	4.65e-02	2.05e+00	14367	158.41632	6.01e-02	2.30e+00	10548	259.30938	1.20e-01	3.26e+00	
		20448	126.80516	2.82e-02	2.58e+00	22188	160.76700	3.67e-02	2.27e+00	15894	265.42276	7.00e-02	2.62e+00	
		31878	128.01394	1.81e-02	2.00e+00	35772	162.61391	2.34e-02	1.89e+00	24162	270.19999	4.36e-02	2.26e+00	
		51735	128.79951	1.17e-02	1.80e+00	57180	163.95736	1.52e-02	1.85e+00	40176	273.62860	2.74e-02	1.83e+00	
		81276	129.40151	7.38e-03	2.04e+00	92091	164.81363	9.74e-03	1.86e+00	65019	276.10676	1.70e-02	1.98e+00	
		131361	129.78774	4.65e-03	1.92e+00	146646	165.36872	6.13e-03	1.99e+00	104229	277.61611	1.06e-02	2.01e+00	
Avg.	*	*	*	2.27e+00	*	*	*	2.22e+00	*	*	*	2.43e+00		
3/4	Perforated cube	18280	67.65476	9.26e+00	*	18280	82.97469	2.05e+01	*	18280	123.46614	1.07e+02	*	
		29940	68.41144	5.87e+00	2.77e+00	34872	84.29090	1.35e+01	1.95e+00	35168	143.63909	1.03e+02	1.84e-01	
		66604	69.31176	3.71e+00	1.72e+00	79500	86.32963	8.77e+00	1.56e+00	49996	151.15309	7.08e+01	3.16e+00	
		150684	70.17242	2.26e+00	1.82e+00	163592	88.27421	5.57e+00	1.89e+00	82652	156.66908	5.82e+01	1.16e+00	
		Avg.	*	*	*	2.10e+00	*	*	*	1.80e+00	*	*	*	1.62e+00

Table 3: Example 2. Convergence history for a variety of 2D and 3D meshes, and different values of κ_0 of the first three eigenvalues $\lambda_{i,h}$. The values of the global total error estimator η_i^2 associated to the i -th eigenvalue ($i = 1, 2, 3$) together with their rate of convergence are also displayed.

Modern jet turbine engines operate by compressing air to very high pressures and temperatures. When this compressed air mixes with fuel and ignites, the resulting hot, high-pressure gases expand through the turbine causing it to rotate and generate the mechanical forces needed to drive the engine. Naturally, the hot gases in the inner chambers of the engine raise the temperature of the turbine blades, which can be damaged when exposed to excessively high thermal loads. To overcome this issue internal air-cooling passages have been previously proposed (see eg. [5, 19]). The air-cooling passages allow the cold air to flow through the engine blades which creates a film that protects the surface from high temperatures.

In this simulation, we consider only the mechanical part of this phenomena with adimensional units, Figure 7 show the domain configuration, including the axial holes acting as the air-cooling

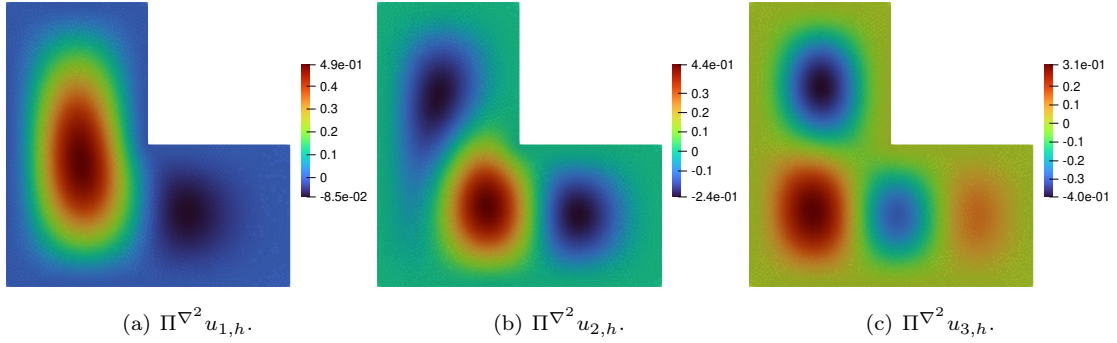


Figure 3: Example 2. Snapshots of the polynomial projection of the first three eigenfunctions in the last refinement step for the L-shaped mesh with $\kappa_0 = 0$.

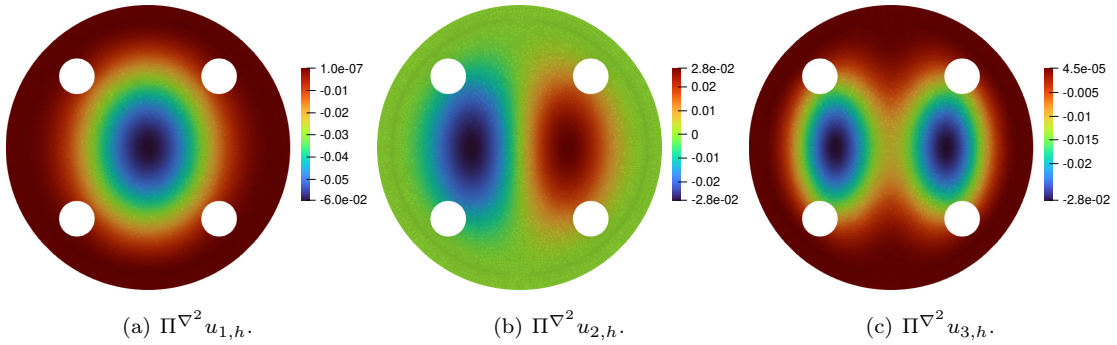


Figure 4: Example 2. Snapshots of the polynomial projection of the first three eigenfunctions in the last refinement step for the perforated circle mesh with $\kappa_0 = \frac{2}{3}$.

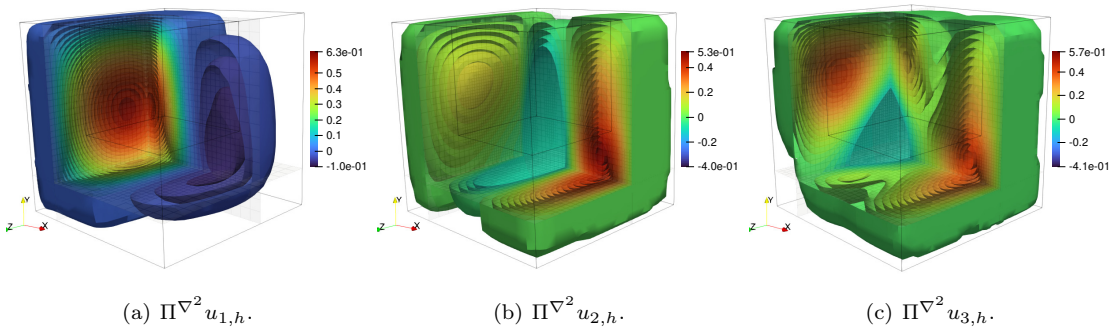


Figure 5: Example 2. Snapshots of the polynomial projection of the first three eigenfunctions in the last refinement step for the perforated Fichera cube mesh with $\kappa_0 = 1$, the isosurfaces are computed from `paraview` starting from the mean value of the projected virtual function on each vertex.

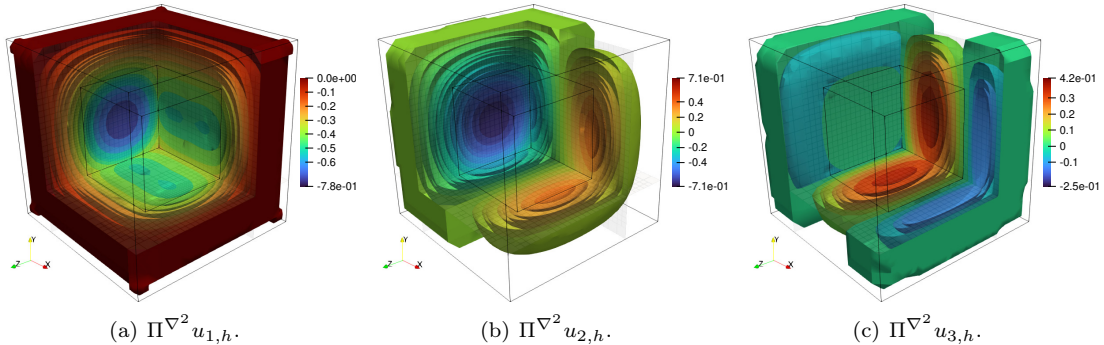


Figure 6: Example 2. Snapshots of the polynomial projection of the first three eigenfunctions in the last refinement step for the perforated cube mesh with $\kappa_0 = \frac{4}{3}$, the isosurfaces are computed from `paraview` starting from the mean value of the projected virtual function on each vertex.

passages. The domain is embedded in the unit square with boundary Γ defined in both the external part of the blade turbine and the axial holes and shear load is imposed, i.e.,

$$\kappa = \begin{pmatrix} 0 & 1 \\ 1 & 0 \end{pmatrix}.$$

We explore the two type of boundary conditions presented in this paper (**SSP** and **CP**), with the material parameters (see [33]) given by $L = 1$, $t = 10^{-3}$, $\nu = 0.3$, and two different cases for the young modulus: room temperature case (298K) with a value of $E = 156\text{GPa}$ and high temperature case (1073K) with a value of $E = 103\text{GPa}$. These parameters correspond to Nickel-based superalloys, typically used in turbine blades and lead to $D = 14.2857$ in the room temperature case and $D = 9.4322$ in the high temperature case. We recall that the effect of the physical parameters relies on the computation of the first non-dimensional critical loading factor $\lambda_{1,h}$.

The critical load factor for each study are reported in Table 4 using the proposed scheme with both uniform and adaptive refinements. The adaptive routine provides very accurate solutions with respect to the uniformly refined, pointing out that approximately 94% fewer degrees of freedom were require to achieve these results. Note that, at high temperature, the turbine blade section's load-bearing capacity decreases by about 34% compared to room temperature. Furthermore, the **CP** boundary condition consistently yields a higher critical load factor than the SSP case at both temperatures, in line with the expected physical behaviour. Finally, snapshots of the associated eigenfunctions are shown in Figure 8.

Acknowledgements

Producto derivado del proyecto INV-CIAS-4321 financiado por la Universidad Militar Nueva Granada - Vigencia (2026)

FD was partially supported by the European Research Council project NEMESIS (Grant No. 101115663). AER has been partially supported by the Australian Research Council through the FUTURE FELLOWSHIP grant FT220100496. IV was partially financially supported by Vicerrectoría

Temperature	Boundary condition	Type of refinement	Refinement iterations	#DoFs	$\lambda_{1,h}$
Room (298K)	SSP	uniform	5	1 009 299	5659
		adaptive	12	46 947	6004
	CP	uniform	5	1 009 299	12632
		adaptive	12	73 956	12640
High (1073K)	SSP	uniform	5	1 009 299	3736
		adaptive	12	46 947	3964
	CP	uniform	5	1 009 299	8340
		adaptive	12	73 956	8345

Table 4: Example 3. Critical load factor for the turbine blade with air-cooling passages (axial holes) at different temperatures under (**SSP**) and (**CP**) boundary conditions, using uniform and adaptive refinement.

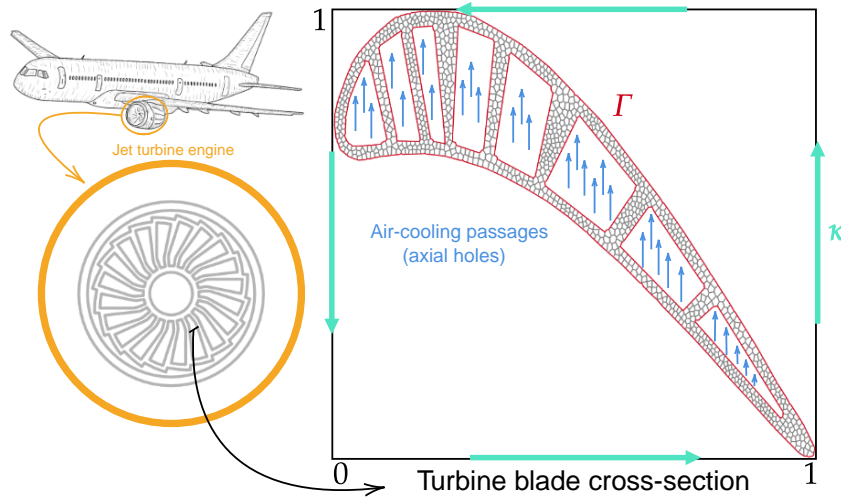


Figure 7: Example 3. Cross-section of a turbine blade with air-cooling passages (axial holes) embedded in the unit square, the effect of the shear load κ and the boundary Γ are highlighted.

de la Investigación de la Universidad Militar Nueva Granada (grant INV-CIAS-4321). We kindly thank Prof. Jesus Vellojin for the support provided in the SLEPC solver implementation.

References

- [1] D. Adak, D. Mora, and I. Velásquez. A C^0 -nonconforming virtual element methods for the vibration and buckling problems of thin plates. *Comput. Meth. Appl. Mech. Eng.*, 403:115763, 2023. DOI: <https://doi.org/10.1016/j.cma.2022.115763>.
- [2] R. A. Adams and J. J. F. Fournier. *Sobolev Spaces*. Elsevier/Academic Press, Amsterdam, Netherlands, 2nd edition, 2003.
- [3] P. F. Antonietti, L. B. da Veiga, S. Scacchi, and M. Verani. A C^1 virtual element method

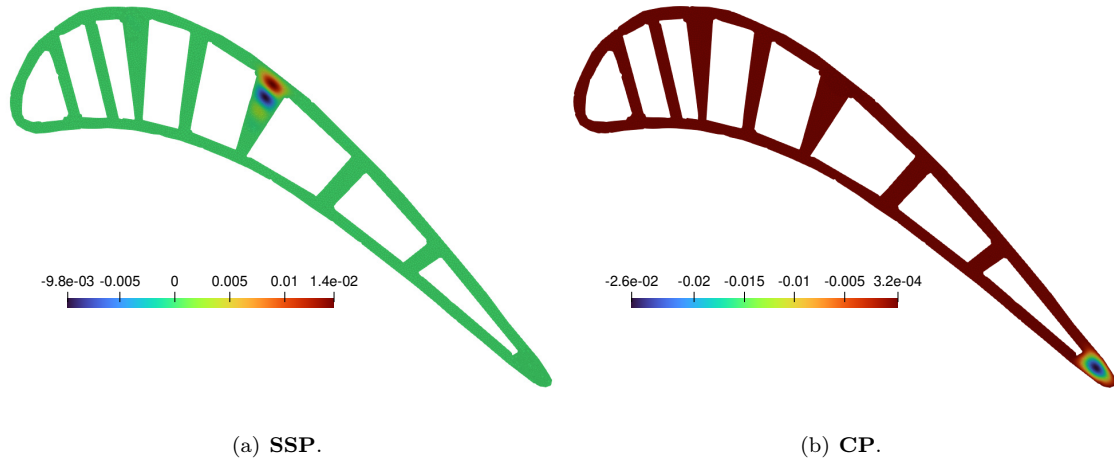


Figure 8: Example 2. Snapshots of the polynomial projection for the first eigenfunctions ($\Pi^{\nabla^2} u_{1,h}$) in the last adaptive refinement step for the turbine blade with air-cooling passages (axial holes).

for the cahn–hilliard equation with polygonal meshes. *SIAM J. Numer. Anal.*, 54(1):34–56, 2016. DOI: <https://doi.org/10.1137/15M1008117>.

[4] S. Badia and F. Verdugo. Gridap: An extensible finite element toolbox in Julia. *J. Open Source Softw.*, 5(52):2520, 2020. DOI: <https://doi.org/10.21105/joss.02520>.

[5] M. Bang, S. Choi, S. M. Choi, D.-H. Rhee, H. K. Moon, and H. H. Cho. Augmented cooling performance in gas turbine blade tip with slot cooling. *Int. J. Heat Mass Transf.*, 201:123664, 2023. DOI: <https://doi.org/10.1016/j.ijheatmasstransfer.2022.123664>.

[6] L. Beirão da Veiga, F. Dassi, and A. Russo. A C^1 virtual element method on polyhedral meshes. *Comput. Math. Appl.*, 79(7):1936–1955, 2020. DOI: <https://doi.org/10.1016/j.camwa.2019.06.019>.

[7] S. C. Brenner, M. Neilan, A. Reiser, and L.-Y. Sung. A C^0 interior penalty method for a von Kármán plate. *Numer. Math.*, 135(3):803–832, 2017. DOI: <https://doi.org/10.1007/s00211-016-0817-y>.

[8] S. C. Brenner and L. R. Scott. *The Mathematical Theory of Finite Element Methods*. Springer, New York, 2008. DOI: <https://doi.org/10.1007/978-0-387-75934-0>.

[9] C. Burstedde, L. C. Wilcox, and O. Ghattas. p4est: Scalable algorithms for parallel adaptive mesh refinement on forests of octrees. *SIAM J. Sci. Comput.*, 33(3):1103–1133, 2011. DOI: <https://doi.org/10.1137/100791634>.

[10] W. Byun, M. K. Kim, K. J. Park, S. J. Kim, M. Chung, J. Y. Cho, and S.-H. Park. Buckling analysis and optimal structural design of supercavitating vehicles using finite element technology. *Int. J. Nav. Archit. Ocean Eng.*, 3(4):274–285, 2011. DOI: <https://doi.org/10.2478/IJNAOE-2013-0071>.

- [11] J. Cao, Z. Wang, W. Cao, and L. Chen. A mixed Legendre-Galerkin spectral method for the buckling problem of simply supported Kirchhoff plates. *Bound. Value Probl.*, 34:1–12, 2017. DOI: <https://doi.org/10.1186/s13661-017-0767-z>.
- [12] C. Carstensen and B. Gräßle. Rate-optimal higher-order adaptive conforming fem for bi-harmonic eigenvalue problems on polygonal domains. *Comput. Methods Appl. Mech. Eng.*, 425:116931, 2024. DOI: <https://doi.org/10.1016/j.cma.2024.116931>.
- [13] P. G. Ciarlet. *The Finite Element Method for Elliptic Problems*, volume 40 of *Classics in Applied Mathematics*. Society for Industrial and Applied Mathematics (SIAM), Philadelphia, PA, 2002. DOI: <https://doi.org/10.1137/1.9780898719208>.
- [14] Ö. Civalek, A. Korkmaz, and Ç. Demir. Discrete singular convolution approach for buckling analysis of rectangular kirchhoff plates subjected to compressive loads on two-opposite edges. *Adv. Eng. Softw.*, 41(4):557–560, 2010. DOI: <https://doi.org/10.1016/j.advengsoft.2009.11.002>.
- [15] F. Dassi. VEM++, a C++ library to handle and play with the virtual element method. *Numer. Algorithms*, pages 1–43, 2025. DOI: <https://doi.org/10.1007/s11075-025-02059-z>.
- [16] F. Dassi, A. E. Rubiano, and I. Velásquez. A posteriori error estimates for a C^1 virtual element method applied to the thin plate vibration problem. *Adv. Comput. Math.*, 52(2):Paper No. 17, 2026. DOI: <https://doi-org.ezproxyucor.unicordoba.edu.co/10.1007/s10444-026-10288-6>.
- [17] F. Dassi and I. Velásquez. Virtual element method on polyhedral meshes for bi-harmonic eigenvalues problems. *Comput. Math. Appl.*, 121:85–101, 2022. DOI: <https://doi.org/10.1016/j.camwa.2022.07.001>.
- [18] J. Feng, S. Wang, H. Bi, and Y. Yang. An hp-mixed discontinuous Galerkin method for the biharmonic eigenvalue problem. *Appl. Math. Comput.*, 450(C), 2023. DOI: <https://doi.org/10.1016/j.amc.2023.127969>.
- [19] Z. Gao, D. P. Narzary, and J.-C. Han. Film cooling on a gas turbine blade pressure side or suction side with axial shaped holes. *Int. J. Heat Mass Transf.*, 51(9):2139–2152, 2008. DOI: <https://doi.org/10.1016/j.ijheatmasstransfer.2007.11.010>.
- [20] F. Gazzola, H.-C. Grunau, and G. Sweers. *Polyharmonic boundary value problems: positivity preserving and nonlinear higher order elliptic equations in bounded domains*. Springer Science & Business Media, Berlin, Heidelberg, 1st edition, 2010. DOI: <https://doi.org/10.1007/978-3-642-12245-3>.
- [21] P. Grisvard. *Elliptic Problems in Nonsmooth Domains*. SIAM, Philadelphia, PA, 2011. DOI: <https://doi.org/10.1137/1.9781611972030>.
- [22] P. Hansbo and M. G. Larson. A posteriori error estimates for continuous/discontinuous Galerkin approximations of the Kirchhoff-Love buckling problem. *Comput. Mech.*, 56(5):815–827, 2015. DOI: <https://doi.org/10.1007/s00466-015-1204-8>.

- [23] V. Hernández, J. E. Román, and V. Vidal. SLEPc: Scalable library for eigenvalue problem computations. In J. M. L. M. Palma, A. A. Sousa, J. Dongarra, and V. Hernández, editors, *High Performance Computing for Computational Science — VECPAR 2002*, pages 377–391, Berlin, Heidelberg, 2003. Springer Berlin Heidelberg. DOI: <https://doi.org/10.1145/1089014.1089019>.
- [24] K. Ishihara. On the mixed finite element approximation for the buckling of plates. *Numer. Math.*, 33(2):195–210, 1979. DOI: <https://doi.org/10.1007/BF01399554>.
- [25] H. Li and Y. Yang. Adaptive morley element algorithms for the biharmonic eigenvalue problem. *J. Inequal. Appl.*, 2018(1):55, Mar 2018. DOI: <https://doi.org/10.1186/s13660-018-1643-9>.
- [26] F. Millar and D. Mora. A finite element method for the buckling problem of simply supported Kirchhoff plates. *J. Comput. Appl. Math.*, 286:68–78, 2015. DOI: <https://doi.org/10.1016/j.cam.2015.02.018>.
- [27] D. Mora and R. Rodriguez. A piecewise linear finite element method for the buckling and the vibration problems of thin plates. *Math. Comput.*, 78:1891–1917, 10 2009. DOI: <https://doi.org/10.1090/S0025-5718-09-02228-5>.
- [28] D. Mora and I. Velásquez. Virtual element for the buckling problem of kirchhoff–love plates. *Comput. Methods Appl. Mech. Eng.*, 360:112687, 2020. DOI: <https://doi.org/10.1016/j.cma.2019.112687>.
- [29] D. Mora and I. Velásquez. Virtual element for the buckling problem of Kirchhoff–Love plates. *Comput. Methods Appl. Mech. Eng.*, 360:112687, 2020. DOI: <https://doi.org/10.1016/j.cma.2019.112687>.
- [30] Mora, David, Rivera, Gonzalo, and Velásquez, Iván. A virtual element method for the vibration problem of kirchhoff plates. *ESAIM. Math. Model. Numer. Anal.*, 52(4):1437–1456, 2018. DOI: <https://doi.org/10.1051/m2an/2017041>.
- [31] R. Rannacher. Nonconforming finite element methods for eigenvalue problems in linear plate theory. *Numer. Math.*, 33(1):23–42, 1979. DOI: <https://doi.org/10.1007/BF01396493>.
- [32] E. Stein, B. Seifert, S. Ohnimus, and C. Carstensen. Adaptive finite element analysis of geometrically non-linear plates and shells, especially buckling. *Int. J. Numer. Methods Eng.*, 37:2631–2655, 1994. DOI: <https://doi.org/10.1002/nme.1620371508>.
- [33] H. Takagi, M. Fujiwara, and K. Kakehi. Measuring young’s modulus of ni-based superalloy single crystals at elevated temperatures through microindentation. *Mater. Sci. Eng. A.*, 387-389:348–351, 2004. DOI: <https://doi.org/10.1016/j.msea.2004.01.061>.
- [34] R. Verfürth. *A Review of A Posteriori Error Estimation and Adaptive Mesh-Refinement Techniques*. Advances in Numerical Mathematics. Wiley-Teubner, Stuttgart, 1996.
- [35] L. Wang, C. Xiong, H. Wu, and F. Luo. A priori and a posteriori error analysis for discontinuous Galerkin finite element approximations of biharmonic eigenvalue problems. *Adv. Comput. Math.*, 45(5-6):2623–2646, 2019. DOI: <https://doi.org/10.1007/s10444-019-09689-7>.

- [36] C. York and F. Williams. Aircraft wing panel buckling analysis: efficiency by approximations. *Comput. Struct.*, 68(6):665–676, 1998. DOI: [https://doi.org/10.1016/S0045-7949\(98\)00050-9](https://doi.org/10.1016/S0045-7949(98)00050-9).
- [37] Y. Yu. Implementation of polygonal mesh refinement in MATLAB, 2021. available at <https://arxiv.org/abs/2101.03456>.
- [38] J. Zhao, S. Mao, B. Zhang, and F. Wang. The interior penalty virtual element method for the biharmonic problem. *Mathematics of Computation*, 92(342):1543–1574, 2023.